RICE UNIVERSITY

Plasmonics of Nanostructures in Planar Geometries
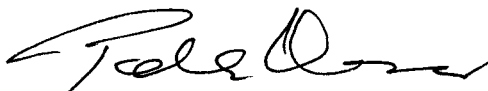
By

Jennifer Marie Steele

A THESIS SUBMITTED
IN PARTIAL FULFILLMENT OF THE
REQUIREMENTS FOR THE DEGREE

Doctor of Philosophy

APPROVED, THESIS COMMITTEE:

Naomi J. Halas, Chair,
Stanley C. Moore Professor of
Electrical and Computer Engineering,
Professor of Chemistry

Peter Nordlander
Director, Rice Quantum Institute
Professor of Physics

Alexander J. Rimberg
Assistant Professor of Physics and
Astronomy, Electrical and Computer
Engineering

Houston, Texas
May 2004

UMI Number: 3122546

INFORMATION TO USERS

The quality of this reproduction is dependent upon the quality of the copy submitted. Broken or indistinct print, colored or poor quality illustrations and photographs, print bleed-through, substandard margins, and improper alignment can adversely affect reproduction.

In the unlikely event that the author did not send a complete manuscript and there are missing pages, these will be noted. Also, if unauthorized copyright material had to be removed, a note will indicate the deletion.

UMI®

Abstract

Plasmonics of Nanostructures in Planar Geometries

By

Jennifer Marie Steele

This thesis presents an experimental and theoretical study of the optical properties for two distinct planer metallic structures: metallodielectric gratings with subwavelength slots and metal nanoshells above a conducting plane. For metallodielectric gratings, two types of anomalies are present in the spectra: an edge anomaly associated with the Rayleigh wavelength, and a resonant anomaly associated with the excitations of surface plasmons. The zeroth-order transmission and reflection were measured to determine the spectral location of these anomalies and their dispersion relationships. The experimental data is compared to theoretical curves calculated using a surface impedance boundary condition approximation. The surface plasmons exhibit an energy gap in their dispersion, which is sensitive to the dielectric properties of the surrounding media. The surrounding media is changed by attaching a second grating to form a crossed grating structure, submerging the gratings in a variety of solvents, or chemically functionalizing the grating. In the first two cases, the plasmon dispersion is shifted to lower energies, the plasmon travel at a slower group velocity, and smaller energy gap is measured. The response of the plasmon dispersion to chemical functionalization is identical, except that the energy gap is increased. The difference in this trend is explained by comparing plasmons traveling on periodic structures to electrons traveling in a periodic potential.

The optical properties of metal nanoshells above a conducting plane are also investigated. When a nanoshell is positioned close to a conducting plane, the surface electrons of the plane will arrange themselves to mimic the electromagnetic field of the nanoshell and its mirror image. This interaction between a nanoshell and its image plasmon approximates a nanoshell dimmer. Transmission spectra are measured as a function of the angle of polarization and compared to the expected spectra of a nanoshell dimer. The thickness of the conducting plane is also varied, which leads to a blue shift in the plasmon resonances. This shift in energy is qualitatively explained by explained using a plasmon hybridization model.

Acknowledgments

"If I have seen further it by standing on the shoulders of giants" – Sir Isaac Newton

I first wanted to be a scientist when I was a little girl, mostly because I wanted to wear the white lab coats. My parents fueled my interest by buying me a cheap microscope and a bee to dissect, and allowed me to grow up in an environment where I was allowed to explore and experiment. Now I hardly ever wear my lab coat, and the one I do wear is tie-dyed, but I have never lost my sense of exploration.

Many people have helped me to this point in my life. First of course my parents, for always supporting and encouraging me. I never felt that there was anything I couldn't achieve. When I arrived at Rice as a confused first year graduate student, Dr. Bill helped me find my way and advised my masters. I then landed in Alex Rimberg's lab. Alex was the first person to teach me how to be a 'real' graduate student with just the right amount of hand holding and letting go. Unfortunately, my project didn't work out, and I found myself coming full circle by being taken in by Naomi Halas, my undergraduate thesis advisor. Naomi showed me not only how to be the best graduate student I could be, but gave me the skills necessary to achieve my career goals. I am truly what I am today because of her guidance. Finally, I have had wonderful theoretical discussions with Peter Nordlander in the later months of my graduate career that have made me truly appreciate the value of talking to theorists during all stages of experiment.

Many of the friends I made here helped me both in scientific and sanity arenas. Cristin Moran has long been a wonderful friend, both in her incredible chemistry

Table of Contents

Table of Figures

Chapter 1: Introduction and Outline

R.W. Wood first observed anomalies in the optical spectra of periodic metallic surfaces in 1902.[1,2] Wood ruled grooves into gold or silver films with diamond scribes to create lamellar reflection gratings. When illuminated with a white light continuum, anomalies consisting of a dark band followed on the low energy side by a bright band appeared in the spectrum. These bands were very sharp, and as the angle of incident light was varied, the dark band split into two bands, one moving up the spectrum and the other down. He also observed that the sharpness of these anomalies could be decreased, or even made to disappear, if the grating was rubbed with a "powder-puff", indicating that the properties of the anomalies not only depended on the period and material of the grating, but the shape of the grooves as well.

The most puzzling aspect of these observations was locating the missing energy from the dark bands in the spectra. A first attempt in explaining these anomalies was made by Lord Rayleigh.[3] He assumed the grating material to be a perfect metal, and found that singularities exist in the electromagnetic field when one diffraction order grazes the surface of the grating as the order becomes evanescent. If the metal is perfectly reflective, the evanescent diffraction order is completely expelled from the metal and travels along the surface. This successfully predicted the frequency, but not the shape of the anomalies. In 1941, Fano considered a more realistic dielectric function for metals in order to obtain a physical picture of the anomalies.[4] He suggested that the

observed anomalies were comprised of two phenomena: an "edge" anomaly at the passing off of a diffraction order (termed a Rayleigh anomaly) and a "diffuse" anomaly associated with the excitation of surface waves, later termed surface plasmons. The experimental and theoretical study of surface plasmon excitations on periodic structures continued throughout most of the century,[5] and was extended to echelette gratings,[6] sinusoidal gratings,[7-9] as well as gratings coated with dielectric materials.[10] Recent experiments and subsequent theoretical analysis concerning the extraordinary transmission through subwavelength hole arrays have focused interest onto the optical properties of metallodielectric or wire gratings.[11-18]

A parallel research path was started by Mie in 1908 through his theoretical calculations of the absorption and scattering of light by small metallic particles.[19] It is now well know that collective oscillations of conduction electrons, or localized plasmons, may be excited in particles with subwavelength length scales.[20,21] Early applications included using gold colloid as an inorganic dye for ruby red stained glass windows. Nanoparticle fabrication techniques have now expanded to allow for a large variety of shapes such as shells,[22] rods,[23] cups,[24] triangles,[25,26] cubes,[27] and disks,[28,29] all with unique plasmon resonances. By manipulating the geometry of the nanoparticles, the plasmon resonance may be tuned from visible wavelengths into the infrared.

Plasmon resonances are accompanied by localized enhancements of the electromagnetic field. The ability to engineer these enhancements has lead to applications such as surface enhanced Raman scattering (SERS)[29-33] and surface plasmon resonance (SPR) sensing.[34-37] Plasmon resonances also have the ability to guide electromagnetic energy on length scales below the diffraction limit.[38] This has lead to

developing metallic nanostructures that can control light at the nanoscale in direct analogy to traditional optical components such as lens, mirrors, and waveguides.[39-41]

Many of these applications rely on a planar geometry in practice. Therefore, understanding how nanoparticles interact with each other, as well as with a substrate, will become increasingly important. However, experimental[42-45] and theoretical[46,47] investigations of nanoparticle-substrate interactions have only just begun. In this thesis, the plasmonics of two nanostructured planar geometries will be explored: metallodielectric gratings with subwavaelength slots and metal nanoshells above a conducting plane. In Chapter 2, surface plasmon excitations on films and gratings will be discussed. An experimental and numerical study of metallodielectric gratings will be presented and both the near and far field of the gratings will be discussed. The wave nature of the surface plasmons will be characterized by their dispersion and band gap. In Chapter 3, the effect of environmental changes to the plasmon dispersion and band gap will be explored. First, microscopic changes to the dielectric medium by chemical functionalization will be compared to macroscopic changes to the dielectric medium by solvent immersion. Then, the results of creating a crossed grating structure will be discussed. How the environment effects the plasmon dispersion and band gap will be compared to electrons traveling through a periodic potential through the Kronig-Penney model. Chapter 4 will explore the optical properties of gold nanoshells suspended above a conducting film. The optical extinction of the nanoshell-film geometry is presented as a function of the orientation of the polarized light and as a function of film thickness. Finally, experimental observation will be qualitatively explained using a plasmon hybridization model.

Chapter 2: Surface Plasmons on Metallodielectric Gratings

2.1 Surface Plasmons on Planar Geometries

Despite being over a century old, both the experimental[9,14,15,48,49] and theoretical[16,17,50-52] study of gratings is still ongoing. Recently, experiments and subsequent theoretical analysis of extraordinary transmission through subwavelength hole arrays[53,54] have focused interest onto the optical properties of transmission or wire gratings. Although transmission gratings have received much theoretical treatment,[17,51,52,55,56] few experimental studies exist.[11,14,50] In this chapter, an experimental and numerical study of surface plasmons (SP) resonances on metllodielectric (silver wire on silica) wire gratings is presented. First, SP resonances on metallic films are discussed as an introduction to SPs. SP excitations on film exhibit the same fundamental properties as SP excitations on gratings and will provide a fundamental understanding of the SP phenomenon. Then, SP excitations on wire gratings will be discussed and a numerical simulation will be introduced. Finally, experimental data will be presented and compared to theory.

2.1.1 Surface Plasmons on Metallic Films

SP excitations on metallic films are collective oscillations of conduction electrons at a metal/dielectric boundary that represent a solution to Maxwell's equations.[5] SP are longitudinal waves that are described by their dispersion $\omega(k_x)$, where k_x is the
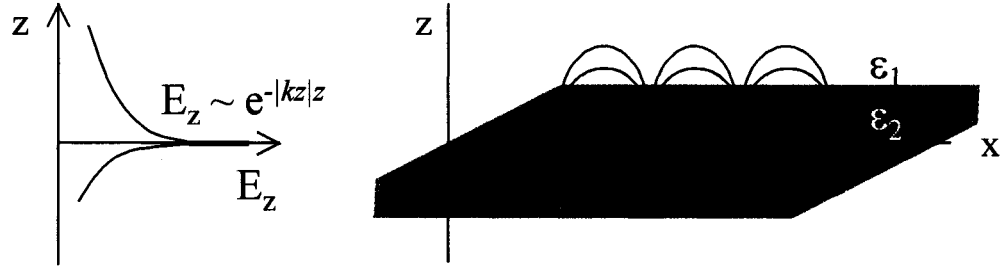
Figure 2.1: Surface Plasmons on Metallic Films

Schematic representation of the charges and electric fields of a SP excitation on a metallic film with dielectric constant ε_2, surrounded by a dielectric medium with ε_1. The SP propagates in the x direction and decreases exponentially in the z direction, as shown on the left.

component of the wavevector tangential to the boundary, as defined in Figure 2.1. In order to derive the dispersion for these surface waves, we look for solutions to Maxwell's equations where the component of the wavevector perpendicular to the surface, k_z, is purely imaginary. No solution can be found for s-polarized light (electric field perpendicular to the plane of incidence), but for p-polarized light (magnetic field perpendicular to the plane of incidence), the fields in region 1 and 2, as defined in Figure 2.1, can be described by the following:

For z>0 $\mathbf{H_1} = (0, H_{y1}, 0)\exp [i(k_{x1}x + k_{z1}z - \omega t)]$

$\mathbf{E_1} = (E_{x1}, 0, E_{z1})\exp [i(k_{x1}x + k_{z1}z - \omega t)]$

For z<0 $\mathbf{H_2} = (0, H_{y2}, 0)\exp [i(k_{x2}x - k_{z2}z - \omega t)]$

$\mathbf{E_2} = (E_{x2}, 0, E_{z2})\exp [i(k_{x2}x - k_{z2}z - \omega t)]$ (2.1.1)

These fields must satisfy Maxwell's Equations:

$$\nabla \times \vec{H}_i = \varepsilon_i \frac{1}{c} \frac{\partial}{\partial t} \vec{E}_i$$

$$\nabla \times \vec{E}_i = -\frac{1}{c} \frac{\partial}{\partial t} \vec{H}_i$$

$$\nabla \cdot \vec{H}_i = 0$$

$$\nabla \cdot \varepsilon_i \vec{E}_i = 0 \qquad\qquad\qquad i=1,2 \quad (2.1.2)$$

and they must also satisfy the continuity relations:

$$E_{x1} = E_{x2}$$

$$H_{y1} = H_{y2}$$

$$\varepsilon_1 E_{z1} = \varepsilon_2 E_{z2} \qquad\qquad\qquad (2.1.3)$$

From the continuity relations follow:

$$k_{x1} = k_{x2} = k_x \qquad\qquad\qquad (2.1.4)$$

It can be derived from Maxwell's equation that the wavevectors must satisfy

$$k_x^2 + k_{zi}^2 = \varepsilon_i \frac{\omega^2}{c^2} \qquad\qquad i=1,2 \qquad (2.1.5)$$

Inspecting equation (2.1.5) along with the localization requirement that k_{zi} be imaginary and taking ε_i to be real, k_x^2 will always be larger than $\varepsilon_i \omega^2/c^2$. SPs therefore cannot transform back into light and are nonradiative.

Taking Maxwell's equations together with the continuity relations, it is possible to derive the following:

$$H_{y1} - H_{y2} = 0$$

$$\frac{k_{z1}}{\varepsilon_1} H_{y1} + \frac{k_{z2}}{\varepsilon_2} = 0 \qquad\qquad\qquad (2.1.6)$$

Which yield the implicit dispersion relation:

$$\frac{k_{z1}}{\varepsilon_1} + \frac{k_{z2}}{\varepsilon_2} = 0 \qquad (2.1.7)$$

Inserting equation (2.1.5) into (2.1.7) yields the explicit dispersion relation:

$$k_{sp} = \frac{\omega}{c}\left(\frac{\varepsilon_1 \varepsilon_2}{\varepsilon_1 + \varepsilon_2}\right)^{1/2} \qquad (2.1.8)$$

Because k_{z1} and k_{z2} were explicitly defined as positive in equation (2.1.1), equation (2.1.7) requires ε_1 and ε_2 have opposite signs. Furthermore, equation (2.1.8) requires $\varepsilon_1 + \varepsilon_2 > 0$. These requirements are fulfilled only if one of the materials is a dielectric and one is either a metal or doped semiconductor. Here, we will assume that ε_1 is the surrounding medium, usually air or another dielectric, and ε_2 is a metal, and therefore will depend on the incident frequency. Additionally, if a Drude dielectric function is assumed for the metal, for large k_x, or when $\varepsilon_2 \rightarrow -\varepsilon_1$, the values of ω_{sp} approaches:

$$\omega_{sp} = \frac{\omega_p}{\sqrt{1 + \varepsilon_1}} \qquad (2.1.9)$$

where ω_p is the plasma frequency for a free electron gas. At large k_x, the group velocity of the SPs goes to zero such that the SP looks like a bulk fluctuation of the electron gas.

The dispersion for a metallic film is plotted in Figure 2.2(a) along with the light line. For small k_x, the SP dispersion approaches the light line. However, as required by equation (2.1.5), the dispersion for SPs always lies to the left of the light line. Therefore, SPs on films cannot be excited by direct optical illumination, and it is necessary to have a

$c/\!sin\theta_0$ c $c/\!\sqrt{\varepsilon_0}\sin\theta_0$ $c/\!\sqrt{\varepsilon_0}$

(a)

(b)
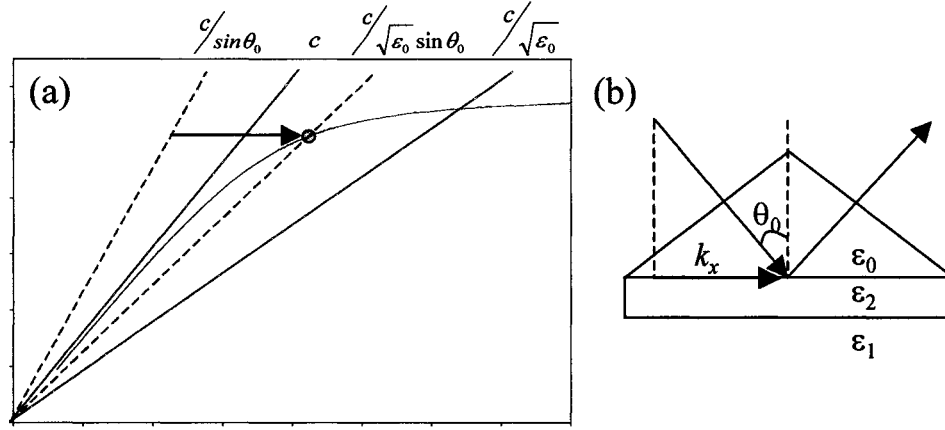
Figure 2.2: ATR Method

(a) SP dispersion for a metallic film (blue). The light line and light line modified by a dielectric with index of refraction greater than 1 are shown in red. SPs are excited using the ATR method: the increased index of refraction depresses the light line such that it intersects the SP dispersion. SPs may be excited up to the point where the SP dispersion intersects the depressed light line. (b) Schematic drawing of the ATR method. The metal, ε_2, is in direct contact with the prism, ε_0 and the SPs are excited through the evanescent field of the totally reflected light along the $\varepsilon_2/\varepsilon_1$ interface. When a SP is launched, energy is coupled into the film and the reflected light is attenuated.

coupling mechanism. The most common coupling mechanism is a prism coupler, known as the Kretschmann-Raether configuration or the attenuated total reflection (ATR) method,[5] shown in Figure 2.2(b). The increased dielectric constant of the silica or other dielectric material, ε_0, depresses the light line such that the light line and the SP dispersion intersect. The projection on the surface of light incident at an angle θ_0 is:

$$k_x = \sqrt{\varepsilon_0}\,\frac{\omega}{c}\sin\theta_0 \qquad (2.1.10)$$

If θ_0 is beyond the critical angle for the boundary of the prism and metal film, the light will be totally reflected, and evanescent waves will be excited along the surface of the metal. SPs may then be excited on the $\varepsilon_1/\varepsilon_2$ interface between the lines of c and $c/(\varepsilon_0)^{1/2}$ as seen in Figure 2.2(a). If k_x matches that of a SP, then energy will be coupled into the

SP and the reflection will be attenuated. SP excitations in this configuration are therefore measured as minima in the total reflection spectra.

Finally, if the metallic films are thin, it is possible for the dispersion to split into high and low energy modes.[5] For a metal film of thickness d with a symmetric dielectric environment on each side, if $k_x d < 1$, the symmetry causes the frequency of the SP to be the same on both sides. There will be both a higher energy mode where the electric field is asymmetric to the z = 0 plane and a lower energy mode where the electric field is symmetric to the z = 0 plane. The splitting of the modes depends on both k_x and d and can be calculated to be the following:[5]

$$\omega^+: \quad \varepsilon_2 k_{z1} + \varepsilon_1 k_{z2} \tanh(k_{z2}d/2i) = 0$$
$$\omega^-: \quad \varepsilon_2 k_{z1} + \varepsilon_1 k_{z2} \operatorname{ctgh}(k_{z2}d/2i) = 0 \tag{2.1.11}$$

Assuming a Drude dielectric function for the metal ε_2, and $\varepsilon_1 = 1$, Equation (2.1.11) yield:

$$\omega^\pm = \frac{\omega_p}{\sqrt{2}}\left(1 + e^{-k_x d}\right) \tag{2.1.12}$$

It is interesting to note that for large k_x, ω_{sp} still approaches $\omega_p/\sqrt{2}$ as in the thick film case.

2.1.2 Surface Plasmons on Periodic Structures

Surface plasmon excitations on periodic structures have the same general characteristics as SPs on films, however, because of the periodicity of the metal/dielectric boundary, SPs may be excited directly on periodic metallic surfaces or gratings. SPs will
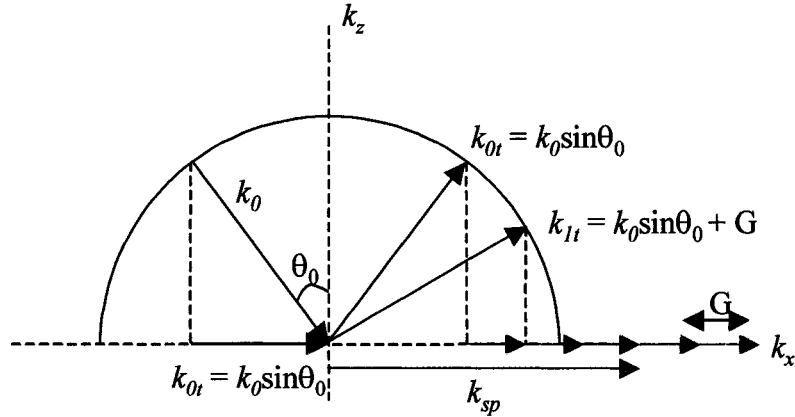
Figure 2.3: Grating Coupler Method

Light with wavevector k_0 is incident on a periodic surface with reciprocal lattice vector G, shown in pink. The periodic surface may redirect or refract the incident light by adding an integral number of reciprocal lattice vectors to the tangential component, k_{0t}. A surface plasmon will be excited if $k_{pt} = k_{sp}$.

be excited on gratings only if the electric field of the incident light is perpendicular to the grooves or wires of the grating. The wavevector of the incident radiation, $k_0 = 2\pi/\lambda$ where λ is the wavelength of the incident light, may be expressed in terms of its component normal to the surface, k_{0n}, and its component tangential to the surface, k_{0t}. The frequency of the incident radiation stays the same, so the grating may only redirect the momentum of the incident radiation, or diffract the light. Therefore, the momentum of any diffracted wave must be equal to $|k_0|$. The normal component of the diffracted wave may take on any value, but the component tangential to the surface may gain momentum in integral multiples of the reciprocal lattice vector, $G = 2\pi/d$, where d is the period of the grating. Therefore, for each diffracted wave of order p, the tangential component of momentum is $k_{pt} = k_{0t} + pG$. The normal component is therefore $k_{pn} = (k_0^2 - k_{pt}^2)^{1/2}$. If $k_{pt} \leq k_0$, then k_{pn} is real and the diffracted order will propagate. However, if $k_{pt} > k_0$ then k_{pn} is purely imaginary and the wave will only propagate along the surface of

the grating and will decay exponentially in the direction normal to the surface, creating a surface wave or SP.

A SP will then be excited if the tangential momentum matches the momentum of the SP:

$$k_{sp} = k_{0t} + \text{pG} = k_0 \sin\theta_0 + \text{pG} \qquad (2.1.11)$$

where k_{sp} is the momentum of the SP and θ_0 is the angle of incidence, as shown in Figure 2.3. When a SP is excited, energy is coupled into the SP and is lost in the remaining propagating orders. This is usually observed as a minimum in the measured spectrum. The SP will either dissipate as heat[11,14] or can also couple back out of the grating by reducing its momentum by pG and reemerging as light.[5]

At normal incidence, only the added momentum from the grating (pG) is available to excite SPs. In this case, two SP's are excited traveling in opposite directions along the grating surface. In direct analogy with photonic band gaps, a plasmonic band gap will result when two counter-propagating SPs interfere to form a standing wave.[14,15,57] This standing wave has two possible field configurations for the same wavevector: one with the maximum field strength concentrated at the metal portions of the grating, and one with the maximum field strength concentrated in the grooves or gaps between wires.[57] Then energy difference between these two standing wave plasmons defines the plasmonic band gap. Since the energy of the SP standing wave depends on the energy stored both in the electromagnetic field and the surface charge distribution,[57] it follows that this energy should be sensitive to the dielectric and chemical properties of

the environment surrounding the grating. Additionally, the grating profile can also affect the energy gap.[14]

When the angle of incidence is varied, this symmetry is broken and the SPs split into two propagating branches, one moving down and one moving up the spectra. By successively rotating the grating and noting the energy of the SP excitation, a dispersion curve, $\omega(k_{sp})$, may be measured for the grating. The dispersion of the grating contains all the physical characteristics of the SP excited on a particular grating, namely the energy of the SPs, the group velocity of the SPs measured from the slope of the dispersion curve, and the magnitude of the plasmonic energy gap.

2.2 Experimental and Numerical Study of Metallodielectric Gratings

The metallodielectric gratings studied in this thesis consisted of silver wires supported on a silica substrate. A typical grating can be seen in Figure 2.4(a). The period of the gratings ranged from 416 nm to 3.3 μm. Typical heights ranged from 25-70 nm, and the slots between the gratings ranged from 70-200 nm. The gratings were fabricated using an all benchtop method developed by C.E. Moran utilizing passivative microcontact printing and eletroless plating.[58] The method produces high-quality, large area periodic metallic structures without the use of lithographic masks and evaporation processing steps. Silica slides are stamped with n-proplytrimethoxysilane (PTMS) using polydimethylsiloxane (PDMS) stamps. The PDMS stamps were molded from commercially available diffraction gratings. The PTMS passivates certain areas of the
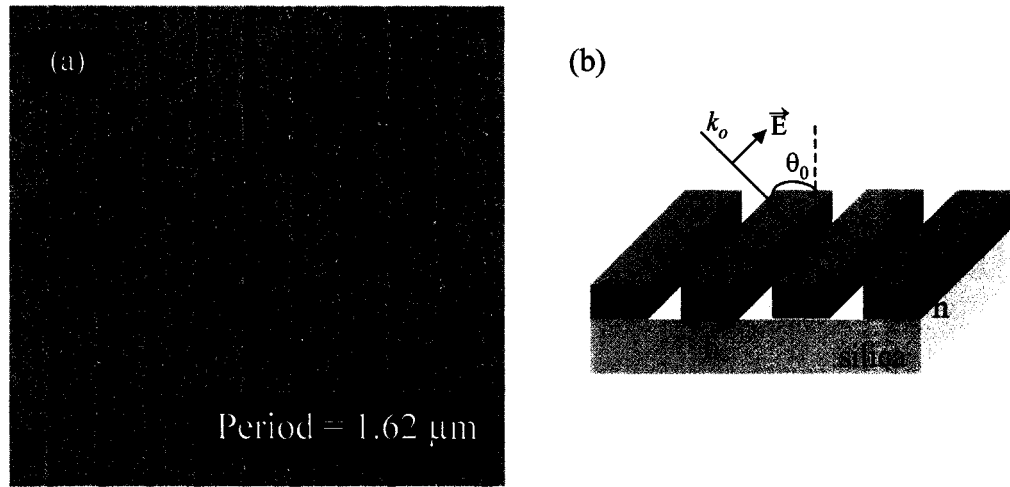
Figure 2.4. SEM Micrograph and Schematic Drawing of Metallodielectric Grating
(a) SEM micrograph of grating. (b) Diagram of the experimental parameters relevant to plasmon excitations on these structures.

slide, which prevents further processing. The exposed surface is then functionalized with a tin precursor. When exposed to a commercially available electroless plating solution, silver reduces onto the tin to form silver wires.

In this work, the samples were illuminated with p-polarized light from a halogen light source. A 0.25-m Jarrell Ash monochromator was used to scan the incident frequency while the sample was held at a fixed angle θ_0, as shown in Figure 2.4(b). Fixing the angle and scanning the incident frequency has been the most accurate way of probing SPs in grating structures.[59] Dispersion curves were measured by successively fixing the incident angle and then scanning the frequency of the incident light. The zeroth-order transmitted or reflected light was collected with a thermoelectrically cooled InGaAs photodiode or silicon photodiode.

2.2.1 Numerical Simulation using a Surface Impedance Boundary Condition

A theoretical method was developed for this system based on an approximate method developed by Lochbihler and Dephine,[60,61] and implemented for this experimental system by A. Lee.[15] Lochbihler and Dephine calculate the fields diffracted by a metallic wire grating for highly conducting metals. The method assumes that the electromagnetic field only penetrates the metal by approximately one skin depth. Instead of calculating the electromagnetic fields inside the metal wires, which is computationally intense, or assuming the metal to be a perfect conductor, which proves inaccurate, the method utilizes a surface impedance boundary condition (SIBC). The tangential components of the electric and magnetic fields are assumed to follow the following condition at the metal/dielectric interface:

$$\mathbf{E}_{||} = Z\mathbf{n} \times \mathbf{H}_{||} \tag{2.2.1}$$

Where $\mathbf{n}$ is a vector normal to the surface, $Z = n^{-1}$, and n is the complex index of refraction of the metal. The electromagnetic fields above the wires are expressed by plane-wave or Rayleigh expansions, and as a modal expansion in between the wires. By combining equation (2.2.1) with Maxwell's equations and matching the fields and their derivatives at the boundaries, the diffracted fields may be solved numerically without intensive computer simulations. The Matlab programs used in this work are described in Appendix A.

2.2.2 Far Field Spectra

Figure 2.5 shows the calculated and measured transmittance for a silver grating with period d = 1.622 μm and a free space width of 172 nm as measured by atomic force microscopy (AFM). The theoretical curve was calculated using the numerical method described above. For all measurements, the light was incident on the air side of the grating. However, the transmission was also measured with the grating turned 180° such that the light was incident on the glass side. The two resulting spectra were identical within experimental error. This was also confirmed by theoretical calculations.

At normal incidence, Figure 2.5 shows two anomalies in the spectra. According to the grating equation for normal incidence, the first diffracted order on the air side become evanescent at an incident wavelength equal to the period of the grating; therefore, a Rayleigh anomaly is expected to occur at 1.622 μm. On the silica side of the grating, the grating equation is modified by the refractive index of the substrate, so the second-order silica side Rayleigh anomaly is expected to occur at 1.23 μm. In both the calculated and measured transmission spectra, a maximum is seen at these wavelengths.

Adjacent to the low energy side of the Rayleigh anomalies a clear minimum in the calculated and measured transmission spectra occurs. These minima also correspond to an increase in the calculated power loss of the transmitted and reflected light.[14] Very little loss of power is expected at the Rayleigh anomalies because as a diffracted order becomes evanescent the energy associated with that order is simply redistributed into the remaining propagating orders. Therefore, the minima in the spectrum can be attributed to SP excitations and the maxima in the spectrum to Rayleigh anomalies.
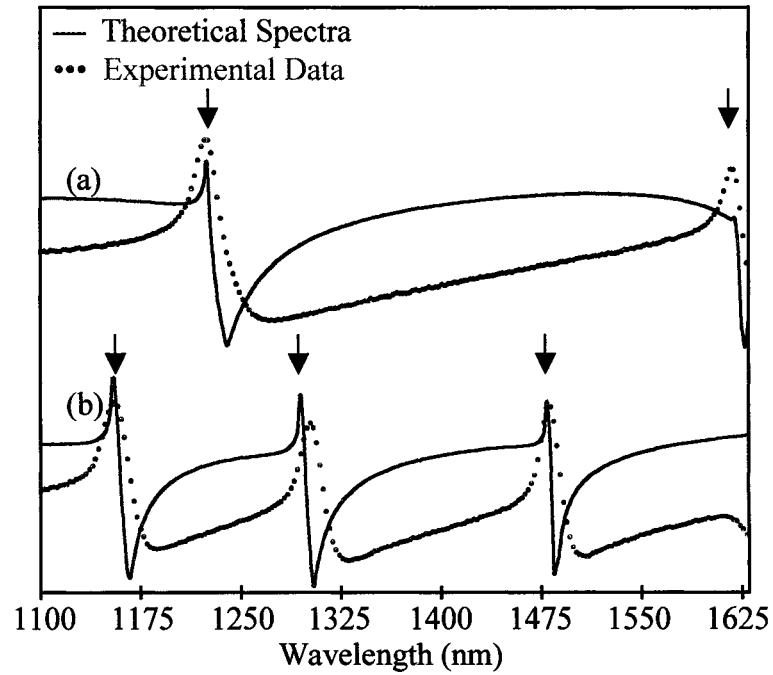
Figure 2.5: Theoretical and Experimental Transmission Spectra

Transmission spectra for a silver grating with a period of 1.62 μm. In (a) the sample is illuminated at normal incidence, and in (b) the sample is rotated 5°. The maxima in the spectra correspond to the Rayleigh anomalies, and their calculated position from the grating equation is marked with arrows. The minima in the spectra can be attributed to surface plasmon excitations.

The measured and calculated spectra are in good agreement considering the limitations of the calculated theory. Two primary differences can be seen between the calculated and measured spectra: first, both the measured Rayleigh maxima and SP minima are broader than what the theory predicts, and second, the SP minima occur approximately 10 nm to the low-energy side of what is predicted by theory. One aspect that contributes to these differences is the idealized shape of the wires that the theory assumes. Because the silver wires are fabricated using electroless plating, they are not perfectly rectangular. The surface roughness can be seen in Figure 2.4. The roughness of the wire surface will add a Δk to the incident light, which will broaden the SP resonance as well as shift its position to a lower energy.[5] Additionally, the theory assumes the electromagnetic field does not penetrate the interior of the wire. This will only be true if the height of the wires exceeds several skin depths. For the grating measured here, the heights varied from 30-60 nm, which is only approximately twice the skin depth of silver. Finally, the dielectric function for silver used in the calculation was based on values measured from bulk silver.[62] Because the silver wires were deposited using electroless plating, it is likely that they have a higher imaginary part of the dielectric function than bulk silver. This would also lead to a broadening of the SP minima. Despite these limitations, the theory adds valuable insight to the physical understanding of the SP excitations observed.

By changing the angle of incidence of the incoming light, symmetry is broken and each pair of SPs splits into a high and low energy branch. This can be seen in Figure 2.5(b) for an incident angle of 5°. The two branches are clearly seen for the second order silver-silica SPs at 1302 nm and 1156 nm. Only the higher energy branch can be seen for

the first order silver-air SP at 1480 nm because the lower energy branch is beyond the range of the detector. As the angle increases, the spectral separation between the SP branches increases. By varying the incident angle of the light and recording the locations of the Rayleigh anomalies and SPs a dispersion curve for these excitations is obtained.

The measured and calculated zeroth order reflectance spectrum for $\theta_0 = 5°$ is shown in Figure 2.6 along with the transmitted spectrum for comparison. What is immediately apparent is the correlation between the spectral features in the reflection spectra and the features in the transmission spectra. At the Rayleigh threshold, there is a minimum in the reflection spectra corresponding to a maximum in the transmission. It is not surprising that the large maximum in the transmittance is accompanied by a large minimum in the reflectance because as a diffracted order becomes evanescent, its energy is not lost, but becomes redistributed into the remaining propagating orders. At the surface plasmon excitations, the minima in transmission correspond to relatively smaller maxima in the reflectance. Because the excitation of a SP results in a loss of power, the overall reflected and transmitted intensity is reduced. As was the case with the transmitted spectra, the measured reflected features are broader and slightly redshifted than what is predicted by the calculated theory. However, the measured spectra matches well with the calculated reflectance, further validating the approximations made in the theory.
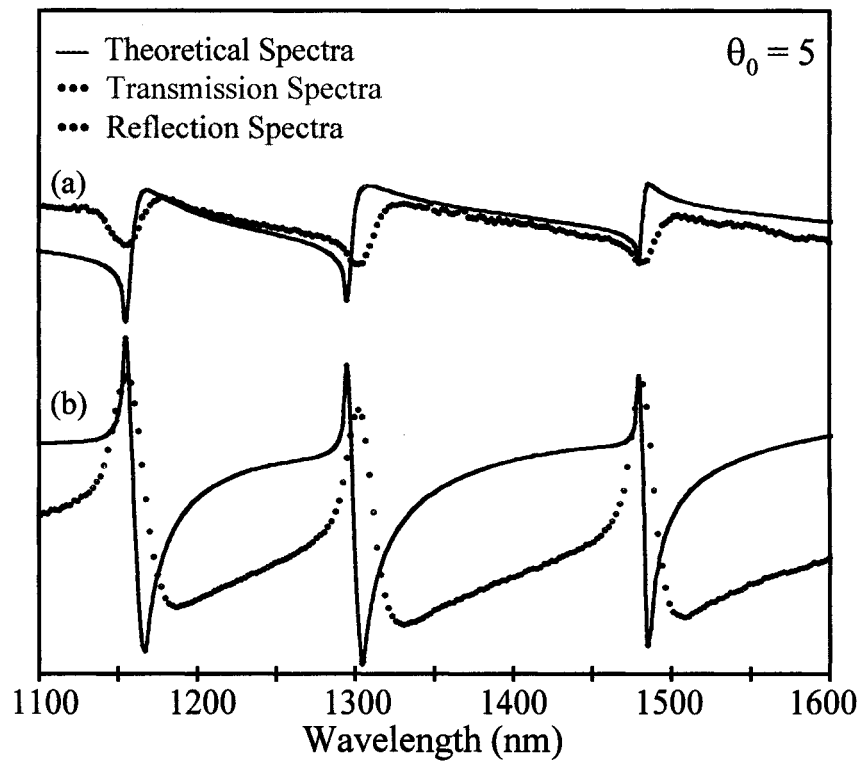
Figure 2.6: Zeroth Order Transmission and Reflection Spectra

Transmission and reflection spectra for an angle of incidence of 5°. (a) shows the reflection spectra and (b) the transmission spectra.

2.2.3 Near-Field Distribution

The differences between Rayleigh anomalies and SP excitations can be seen quite dramatically in the near field distribution of the electric field above and below the silver wires. In Figure 2.7, the near field intensity of the y-component of the electric field is plotted in the vicinity of the grating surface as calculated using the SIBC approximation previously described. The white rectangles are the cross sections of the silver wires. The grating used in the calculation has the same parameters as the experimental grating discussed in Section 2.2.2. The light is incident from the top and the silica substrate is below the wires. The plots extend 5.5 μm from the top and bottom surface of the wires. Because the media above and below the wires is not the same, the electric field intensity is quite different on either side. Figure 2.7(a) and (b) show the features associated with the first diffracted order on the silver-air side of the wires, where (a) is the near field distribution at the Rayleigh anomaly and (b) is the near field distribution of the SP excitation. Figure 2.7(c) and (d) show the corresponding near field distribution of the features associated with the second diffracted order on the silver-glass side of the wires. The color scale is the same for all graphs.

For the first diffracted order features, (a) and (b), there are two lobes on each wire. However, for the second diffracted orders, (c) and (d), there are four lobes on each wire because the wavelength of the second order excitations are half as long as the wavelengths of the first diffracted order excitations. The intensities of the fields for the second diffracted order features are not as large as the intensities of the first diffracted
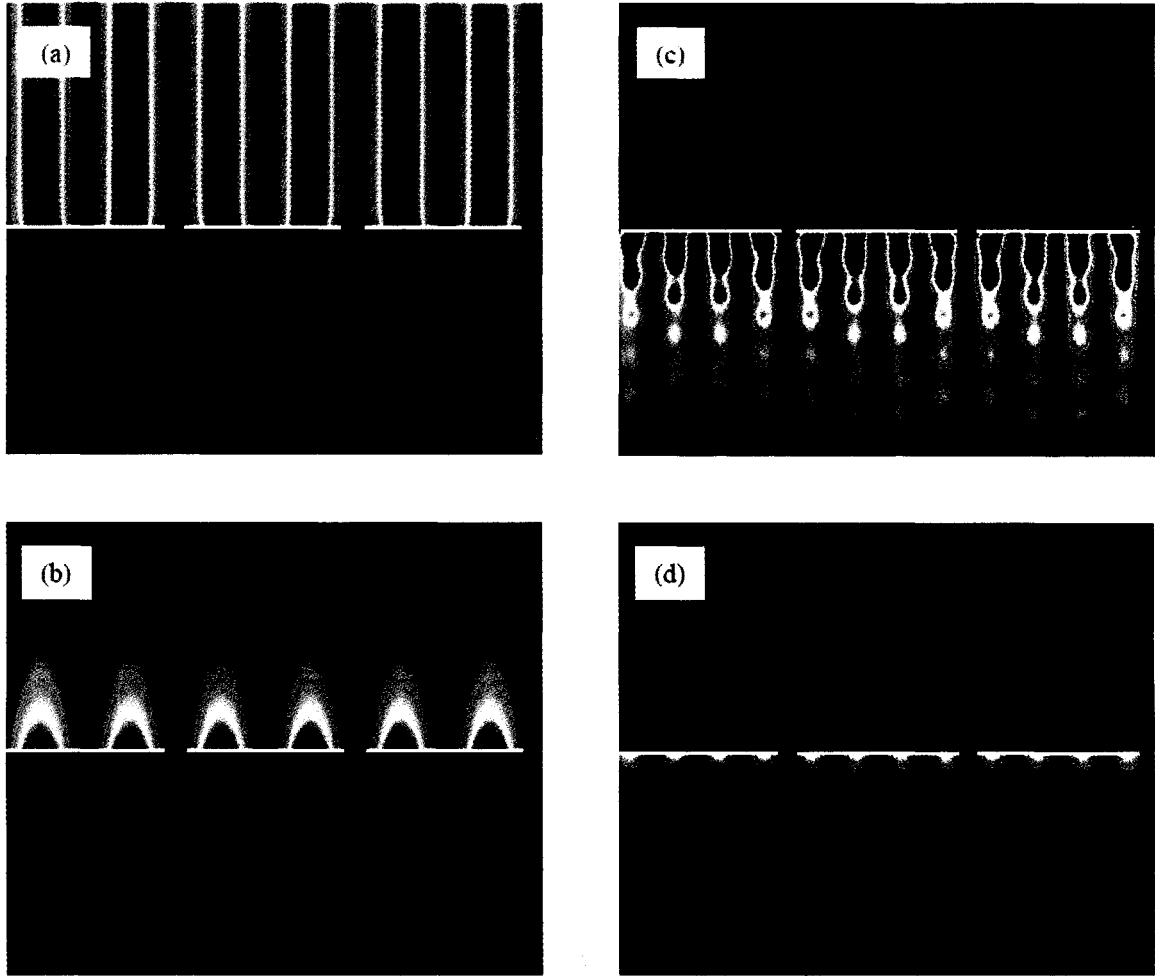
Figure 2.7: Near Field Plots of SP Excitations and Rayleigh Anomalies

Graphs showing contour plots of $|E_y|^2$. The cross section of the wires is shown as white boxes. The light approaches at normal incidence from the top. The upper region is the air side of the grating and the lower is the silica side. The plots extend 5.5 μm from the surface of the wires. The period of the grating is d = 1.62 μm with a free space gap of 172 nm. The color scale is consistent for all four plots. (a) is the first order silver-air Rayleigh anomaly, (b) is the first order silver-air side plasmon, (c) is the second order silver-silica side Rayleigh anomaly, and (d) is the second order silver-silica side plasmon.

order features. Additionally, in the second diffracted order Rayleigh anomaly (c), there is an envelope function that follows the wire grating structure. This structure appears as the electric field expands into the free spaces between wires that causes a beating oscillation in the electric field. It is interesting to note that even though the free space between the wires is very small relative to the rest of the grating parameters, it still has significant effects on the near field distribution.

The near field distributions for the SP excitations are bound to the metal/dielectric interface and do not extend into the free space between the wires. This is similar to what was reported by Popov et al.[55] while examining cavity and SP resonances in deep wire gratings. Their calculations showed that for SP excitations, the enhancement in the near field distribution was concentrated at the metal/dielectric interface, but not between the wires themselves. This is not the case for cavity modes that can be excited in between the wires if the grooves are deep enough.

Another apparent difference in the near fields of the Rayleigh anomalies and the SPs is the distance the enhanced electric field extends from the grating surface. For the Rayleigh anomalies, the enhancement of the electric field extends far from the grating surface because Rayleigh anomalies are still propagating waves. Because SPs are surface waves, the electric field intensity decreases exponentially with distance from the grating. This is a distinction that may prove to be important in possible applications of these gratings to sensing. For example, if the surface of the gratings is chemically functionalized or modified, it is likely that only the SP dispersion will be modified because most of the field of the SPs is close to the surface of the structure. However, if

the properties of the embedding medium are changed, the dispersion of both the Rayleigh anomalies and SPs are likely to change in response.

Figure 2.8 shows the Poynting vector for the same excitations as Figure 2.7. The length of the arrows is proportional to the energy at each point, and all four plots are equally scaled. The grating used has a period d = 1.6 μm and a free space gap of 200 nm. The plots show only one period to illustrate the energy flow in the vicinity of the slots. As in Figure 2.7, light is incident from the top, the glass side is on the bottom, and the cross sections of the wires are shown as grey boxes. Looking at the energy flow for the Rayleigh anomalies for the air and glass side excitations shown in (a) and (c), it is clear that energy is squeezed through the slot. This is to be expected since the Rayleigh anomalies correspond with and increase in transmission. For the silver-air and silver-silica interface SP's shown in (b) and (d), it is apparent that the energy primarily flows parallel to the grating with very little transmitted energy. Additionally, some of the energy becomes trapped in the vortices formed on the incident side of the grating, resulting in the minima observed in the transmission.
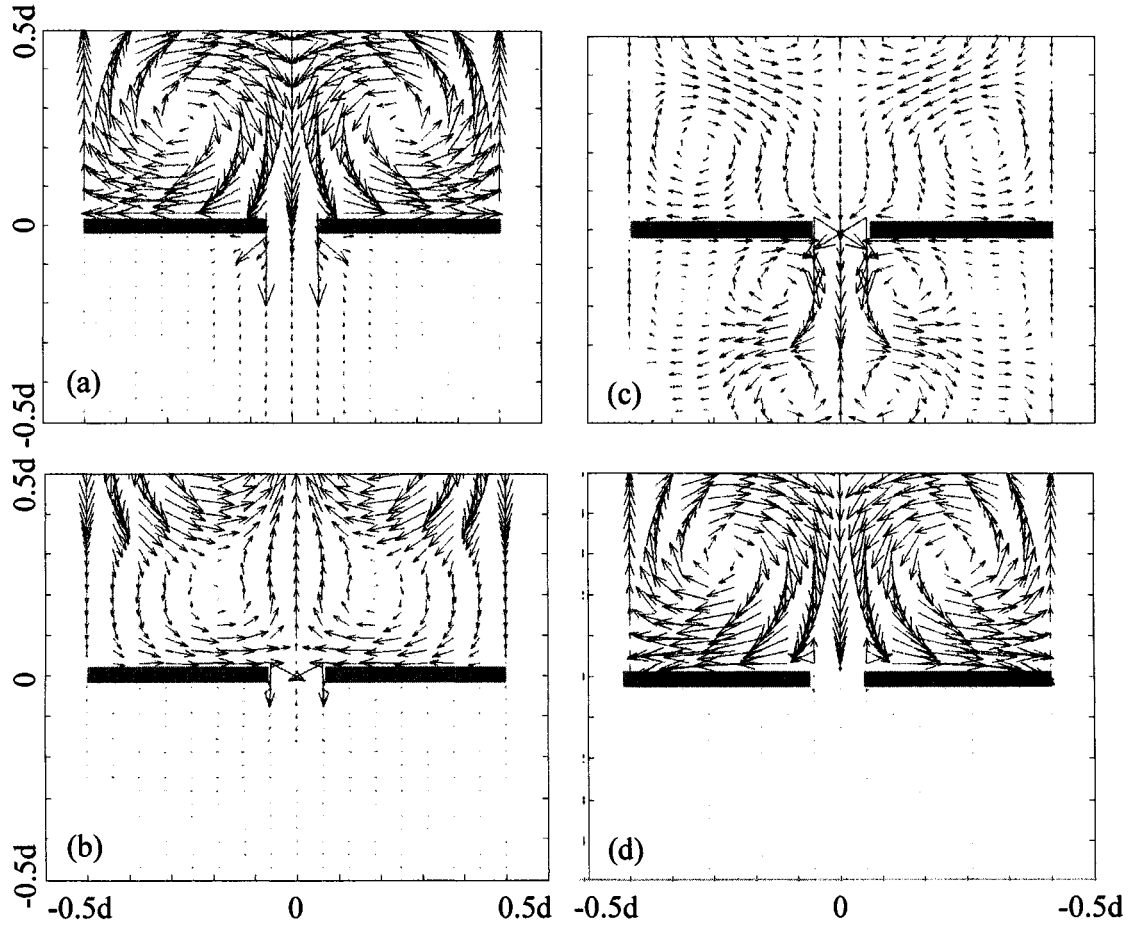
Figure 2.8: Poynting Vector Plots of SP Excitatoins and Rayleigh anomalies

Poynting vector plots of the electromagnetic field in the immediate vicinity of the gaps. The grating has a period d = 1.6 μm and a free space gap of 200 nm. Orientation is the same as Figure 2.7, but here only one period is shown and the plot extends 0.5d from the top and bottom of the wires. (a) and (c) show the energy flow for the Rayleigh anomalies for the silver-air and silver-glass side excitation respectively. (b) and (d) show the energy flow for the SP excitations for the silver-air and silver-glass side excitations respectively.

2.2.4 Dispersion

The dispersion curve of the second order silica side spectral features for the same grating discussed in Section 2.2.2 is shown in Figure 2.9. The Rayleigh anomaly maxima are plotted as crosses, and the SPs minima as diamonds. The spectral positions of the Rayleigh anomalies and SPs were determined by holding the incident angle constant while sweeping the incident frequency. The range of angles used was -10 to +10 degrees. The Rayleigh threshold for the second diffracted order on the silica side to become evanescent is plotted as a straight line using the grating equation. As expected, the Rayleigh anomalies do not disperse from this threshold. It is interesting to note that where the plus and minus second order Rayleigh anomalies cross, a small energy gap does appear. Rayleigh anomalies are not traveling waves bound to the surface like SPs, but occur when a diffracted order skips along the grating surface. At normal incidence when the incident light has the same wavelength as the grating period, the plus or minus first diffracted orders both graze the grating surface at the same time. It is therefore possible that they interfere and an energy gap appears.

The surface plasmons clearly disperse from the Rayleigh threshold, and the amount of dispersion increases as the excitation energy increases. Although this result is not unexpected, it is different than what was reported by Lochbihler for gold wire gratings.[14] The main difference between the structures examined here and the ones studied by Lochbihler is the width-to-period ratio, b/d, which ranged from 0.2-0.5 whereas in this study b/d = 0.89. The gratings studied here more closely resemble a silver film, so it is not surprising that the dispersion from the Rayleigh threshold
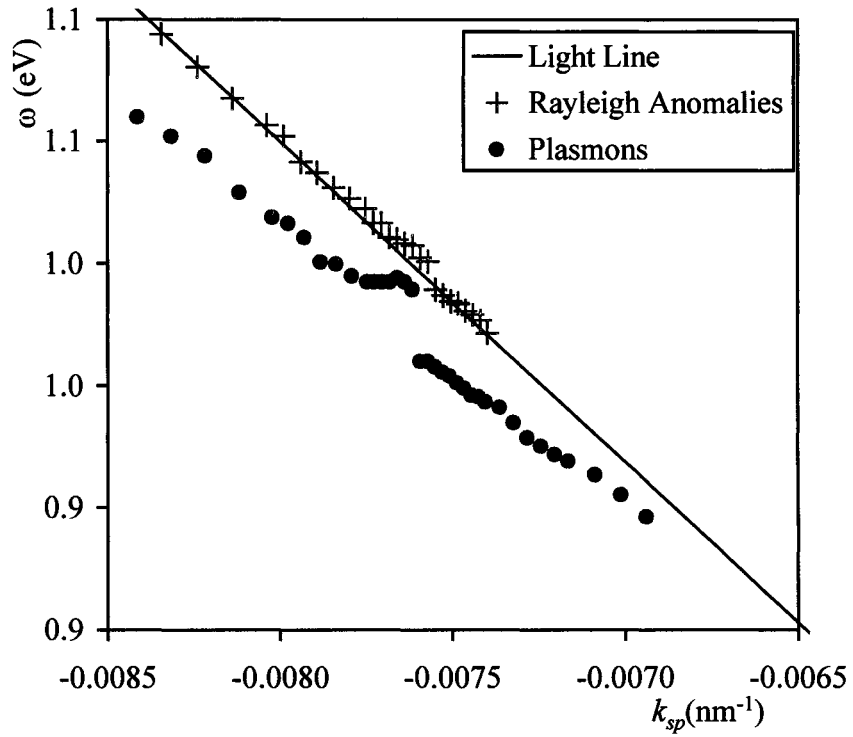
Figure 2.9: Dispersion of SP and Rayleigh Anomalies

Dispersion relationship of the SPs and Rayleigh anomalies. Rayleigh anomalies do not disperse from the light line, while SPs disperse and show a plasmonic energy gap where two plasmons are excited at the same energy.

increases with increasing energy as is the case for films.[5] These results are also similar to the work by Schroter and Heitmann performed on thin modulated silver films[9]. They observed both maxima and minima in the transmission spectra of their films. The maxima did not disperse significantly from the Rayleigh thresholds and a small energy gap appeared at the crossings. However, the minima dispersed further from the Rayleigh thresholds and had a larger energy gap.

A large energy gap of 29.7 ± 2.5 meV occurs where the plus and minus second order SPs are excited with the same frequency on the silver-glass interface of the grating. An energy gap also appears when two different plasmons are excited at the same frequency on opposite sides of the grating, similar to thin metallic films. Figure 2.10 shows the dispersion for SP excitations on a silver grating with a period of 1.622 μm and a free space width of 172 nm. At normal incidence, the expected plasmonic energy gap is measured to be 29.7 ± 2.5 meV as shown in Figure 2.10(a). A second smaller energy gap of 14.4 ± 2.6 meV appears when the +1 silver-air side plasmon is excited at the same frequency as the silver-silica side plasmon as shown in Figure 2.10(b). This energy gap is about half of the energy gap created when both SP are propagating on the same side of the grating, indicating the coupling between SPs on opposite sides of the gratings is weaker than when the SPs are excited on the same side of the grating.
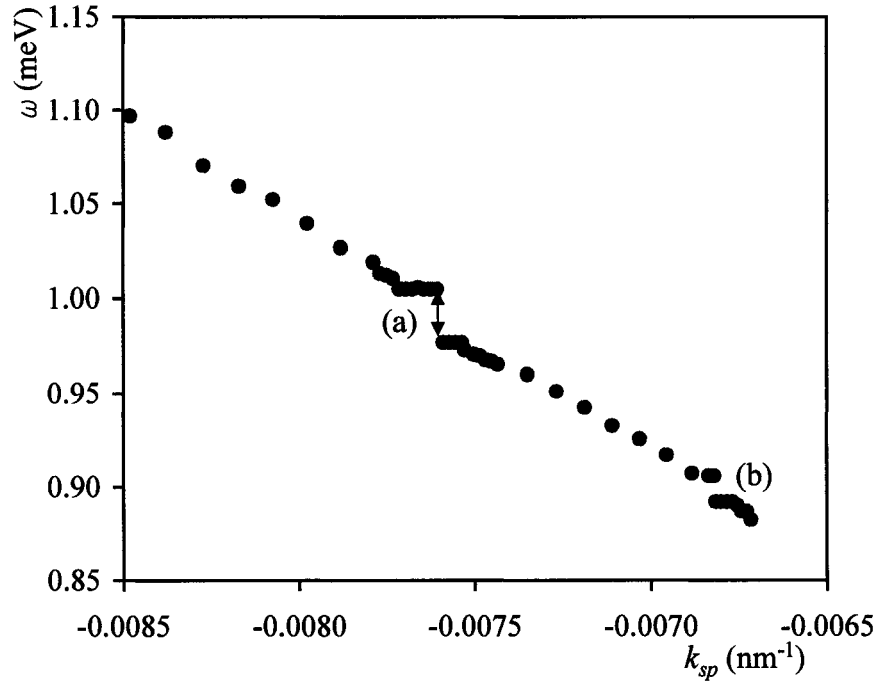
Figure 2.10: Dispersion for Surface Plasmons

Dispersion curve showing energy gaps where plasmons are excited on both the same and opposite sides of the gratings. (a) A gap of 29.7 ± 2.5 meV is created when the ± 2nd order silver-silica side plasmons are excited at the same frequency. (b) A gap of 14.4 ± 2.6 meV is created when the +1 silver-air side plasmon and the –2 silver-silica side plasmon are excited at the same frequency.

2.3 Discussion and Summary

This chapter discusses the surface plasmon (SP) excitations on metallic films and metallodielectric gratings. SPs are collective oscillations of electrons along a metal/dielectric boundary. Their dispersion lies outside the light cone, so they may only be excited by using the Kretschmann-Raether configuration or by having a periodic modulation along the surface of the metal. Theoretical calculations and experimental measurements were made on silver metallodielectric gratings. The theoretical calculations match both the transmitted and reflected spectra well. Near field plots and the Poynting vector were also calculated to give physical insight to the different excitations. For the Rayleigh anomalies, the near field plots showed a large, unbounded electromagnetic wave and the Poynting vectors indicate that energy was squeezed through the slots between the wires. For SPs, the near field plots showed a bound surface wave and the Poynting vectors show that energy was mostly directed along the surface of the metal wires with very little propagating through the slots between the wires.

The SPs were characterized by plotting their dispersion. A plasmonic band gap was found when two SP were excited when the incident light was normal to the surface and two plasmons were excited at the same frequency. Additional band gaps were found when two SPs were excited on opposite sides of the grating, indicating that the gratings are thin enough to allow modes on opposite sides to couple together. Now that the basic SP characteristics are known, the next chapter will focus on manipulating the SP dispersion by changing the surrounding dielectric medium of the wire gratings.

Chapter 3: Response of Surface Plasmons to Environmental Changes

Although the electromagnetic fields of surface plasmons (SPs) decay exponentially in directions normal to the surface of the metal, the skin depth extends far enough to make surface plasmons sensitive to changes in the surrounding medium. Because of this sensitivity, metallic films have been utilized in applications such as surface plasmon resonance (SPR) sensing.[36,63-65] SPR sensing tracks chemical reactions by measuring changes in the SP energy in response to chemical binding events on the surface. Because of the relatively long range of SP near fields in the surrounding medium, it is possible to track several binding events. Typical skin depths for the SPs excited on a silver film range from about 400 nm for wavelengths in the visible to over 4 μm in the near IR.[5]

Recently nanoparticles either suspended in solution or immobilized on a surface have also been utilized as SPR substrates because of the nanoparticles' sensitivity to changes in their dielectric mediums.[27,36,66] Additionally, SPs can be excited on nanoparticles without a coupling mechanism, giving an advantage over metallic films. However, because the SPs excited on particles are localized, the only measurable experimental parameter is the SP's energy. The metallodielectric gratings in this work combine the best features of both metal films and metal nanoparticle substrates because gratings support SP waves that propagate along their surface, unlike the localized SP excitations of metal nanoparticles.[5] Additionally, due to its periodic structure,

momentum matching of the incident optical wave and the surface plasmon becomes possible, resulting in direct optical excitation of surface plasmons without the need of a prism coupler. By monitoring the energy at which an SP is excited, the group velocity of the SPs, and the energy and magnitude of the plasmonic band gaps, one can quantitatively examine how the surrounding medium modifies the character of the SPs.

In this chapter, the response of SPs to physical dielectric changes will be explored. First a crossed grating geometry is examined by placing a second wire grating in close proximity to a first such that the wires are perpendicular to each other. This introduces a periodic metallodielectric surrounding medium. Additionally, the effect of changing the macroscopic dielectric environment by solvent immersion will be compared to changing the microscopic chemical environment through chemical functionalization.

3.1 Chemical and Dielectric Manipulation of the Plasmonic Band Gap

Changes both in the surrounding dielectric medium and chemical environment of the metallodielectric gratings were explored. The surrounding dielectric medium is changed macroscopically by immersing the gratings in solvents with different dielectric constants, as shown schematically in Figure 3.1(a). Chemical modifications of the gratings are accomplished by functionalizing the silver wires with different alkanethiols, shown Figure 3.1(b). For this study, gratings with a period of 555 nm are fabricated with a wire height of approximately 30 nm using the passivative electroless plating method described in Chapter 2. Throughout both solvent immersion and chemical functionalization, the gratings proved to be mechanically robust and showed no evidence of degradation.
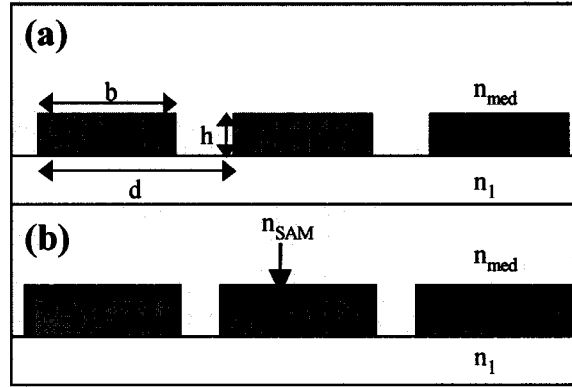
Figure 3.1: Schematic drawing of changes to surrounding dielectric medium.

(a) Gratings with period, d, wire width, b, and wire height, h, were fabricated on glass substrates (n_i). Changes to the bulk dielectric environment, n_{med}, were made by immersion in a variety of solvents. (b) Changes to the nanoscopic dielectric environment around the wires, n_{SAM}, were made by functionalization with alkanethiol SAMs.

Figure 3.2(a) shows the zeroth order transmission spectra at normal incidence for a grating both in (i) air and (ii) water. The -1st order plasmon appears as a minima in the spectrum at 600 nm in air. When immersed in water, the SP shifts to 798 nm in response to the index of refraction of the surrounding medium (n_{med}) increasing from 1 to 1.33. Figure 3.2(b) shows the plasmon dispersion for the same grating in air and immersed in water, and three trends can be observed. First, the SP dispersion is depressed to lower energies in response to the higher index of refraction. Second, the group velocity of the SPs as measured by the slope of the dispersion decreases from 0.83c to 0.72c, where c is the speed of light, indicating that the silver-air plasmons travel along the grating faster than the silver-water plasmons. Third, the energy gap decreases from 139 ± 7 meV in air (Figure 3.2(b)(i)) to 88±4 meV in water (Figure 3.2(b)(ii)). Dispersion curves were also measured for a single grating immersed in a variety of solvents with indexes of refraction ranging from air, n_{med} = 1, to carbon disulfide, n_{med} = 1.65. Representative data in Table

3.1 reveals that as the index of refraction of the surrounding medium increases, the plasmonic energy gap decreases.

These results are compared to experimental data taken by C.E. Moran[67] by functionalizing the gratings with alkanethiols. The transmission spectra and dispersion of gratings with a period 555 nm functionalized with dodecanethiol or hexadecanethiol was measured. The gratings were functionalized by immersion in a 1 mM ethanolic solution of thiol for 12 hours and the spectra were measured immediately upon removal from solution. The alkanethiols used in this study extend about 2 nm from the grating surface, which is much smaller than the physical extent of the SP's near field[5,15] as shown in Figure 2.7. However, the energy of the SP still shifts on average 30-50 nm, which is similar to the shifts observed for metal nanoparticles coated with alkanethiol molecules.[36] Figure 3.2(c) shows the transmission of a grating as made and after functionalization with dodecanethiol. The SP for the bare grating is excited at 596 nm (i), and shifts to 632 nm with the addition of dodecanethiol (ii).

The dispersion for the -1st order plasmon is shown in Figure 3.2(d). There are two similarities to the solvent case. First, the SP excitations are depressed to lower energies as if the surrounding index of refraction was increased. Second, the group velocity decreases form 0.81c to 0.73c as in the solvent case. But, in direct opposition to the observed solvent immersion trends, the energy gap increases with functionalization. For the bare grating, the energy gap was measured to be 64 ± 3 meV (i), but for the same grating functionalized with dodecanethiol, the energy gap increases to 152 ± 8 meV (ii), as seen in Figure 3.2(d) and Table 3.1. This unexpected result indicates that the bound molecules do not act simply as a thin dielectric layer, in which case a decrease in the
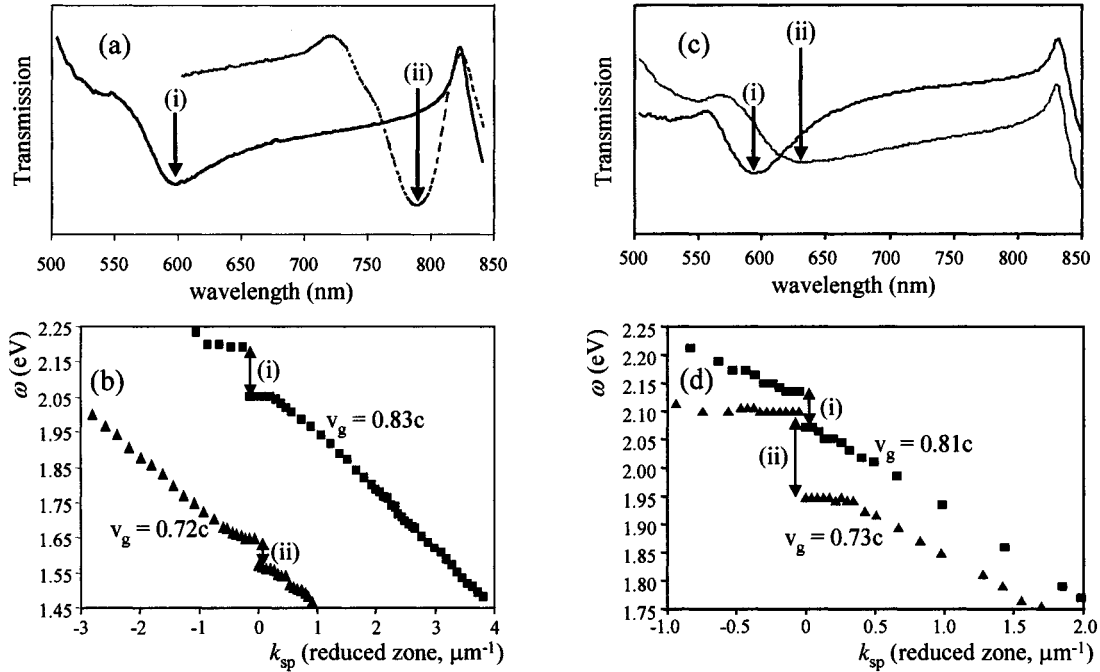
Figure 3.2: Chemical and dielectric manipulation of surface plasmons

(a) Zeroeth order transmission spectra at $\theta = 0°$ showing the -1st order SP shift from 600 nm in air (i) to 789 nm in water (ii). (b) Dispersion relations of the -1st order SP propagating in air (squares) and water (triangles) show a decrease in the energy gap size with increasing index of refraction of the medium, from 139 ± 7 meV in air (i) and decreases to 88 ± 4 meV in water (ii). (c) Zeroeth order transmission spectra at $\theta = 0°$ showing the -1st order SP. (i) shows the SP for the bare grating at 596 nm, and (ii) shows the SP shifting to 632 nm due to the addition of dodecanethiol (DDT). (b) Dispersion relations of the -1st order SP for a grating modified with a SAM measured in air. The dispersion curve for the bare grating (squares) show an energy gap of 64 ± 3 meV (i), and the dispersion curve for the same grating functionalized with DDT (triangles) show the energy gap increasing to 152 ± 8 meV (ii).

Table 3.1: Plasmonic energy gaps for different solvents and molecular functionalization

Measured energy gaps for a single grating immersed in several solvents and a second grating functionalized with different alkanethiols. The difference in energy gap in air between the two samples is due to slightly different roughness and grating parameters

Solvent	Index of Refraction	Energy Gap
Air	1	90.6 ± 5 meV
Water	1.33	56.7 ± 3 meV
Ethyl Alcohol	1.36	55.0 ± 3 meV
Isopropanol	1.38	55.8 ± 3 meV
Carbon Disulfide	1.61	16.5 ± 2 meV
Molecule	Carbon Chain Length	Energy Gap
Bare	-	64 ± 3 meV
Dodecanethiol	12	152 ± 6 meV
Hexadecanethiol	16	160 ± 7 meV

energy gap is expected. Modifying the surface chemistry of the silver wires must also affect the SP, and therefore the plasmonic band gap, through some other mechanism.

Because the problem of SP propagation along a grating is complex, deriving a theoretical model that predicts the response of the energy gap to changes in the dielectric medium is impossible without significant approximations. One such effort was made by Barnes *et al.* for thin sinusoidal gratings where it was found that the size of the energy gap was inversely proportional to the index of refraction of the surrounding medium.[57] To derive an analytical expression for the plasmonic energy gap, they used the Chandezon technique, which transforms the coordinate system such that the periodic interface is flat. By expressing Maxwell's equations in the new coordinate system, solutions for surface waves along the metal/dielectric boundary are found and then transformed back into Cartesian coordinates. It was found that the magnitude of the energy gap was inversely proportional to the index of refraction of the surrounding medium.[57] This correctly predicts the trend observed by solvent immersion (Table 3.1). However, this approach makes no predictions concerning how chemical functionalization will change the SP energy.

To understand how changes in the surrounding dielectric media or chemical functionalization affect the SP propagation characteristics observed in the experiments described above, plasmons traveling along a periodic metallic surface are compared to electrons propagating in a periodic potential using the Kronig-Penney model.[68] Without explicitly defining the shape of the periodic potential, the model predicts that as the potential barriers increase, the energy gap also increases, and vice versa. If we consider the metal wires and air gaps between the wires as areas of low and high potential, we may

make some predictions on how changing the dielectric functions of the surrounding media or molecular functionalization will affect the energy gaps.

If the area between the wires is filled with a dielectric with $n_{med}>1$, then, similar to a parallel plate capacitor, the potential required to induce a surface charge density on the wire surfaces will be lowered. It is therefore expected that the energy gap will decrease with increasing n_{med}, which agrees with experimental observations. In the case of molecular functionalization, it is clear from the experimental data that the SAM cannot be thought of as only a thin dielectric layer. Although the energy of the SP excitation is reduced as if n_{med} increases (see Figure 3.2(c)), because the energy gap increases (see Figure 3.2(d)), there is evidence that there are two competing processes: a chemical effect due to the sulfur-Ag bond and an electromagnetic effect from the index of refraction of the molecule itself. The chemical effect is due to a partial charge transfer to the metal through the sulfur-metal bond.[69-71] Although electrons are added to the metal in this process, it is quite plausible that the surface impedance of the metal increases at the optical frequencies relevant to plasmon propagation because of the participation of electrons in localized chemical bonds with the sulfur.[36] Increasing the potential barrier should increase the energy gap, corresponding to our experimental observations. The accompanying dielectric properties of the surrounding SAM may be sufficient to cause the observed SP redshift and reduction of group velocity, as seen in the case of the bulk embedding medium.

3.2 Crossed Gratings

By attaching a second grating perpendicular to the first, a crossed grating structure may be investigated. The metallodielectric gratings used in this experiment have a period of 577 nm, a silver wire width of about 480 nm, and a height of about 40 nm. The dispersion curve for the first order air side SP is shown in Figure 3.3. Two gaps are evident in the dispersion. The gap centered at 2.24 eV occurs at normal incidence, where the first order air side plasmons interfere. The energy gap that results is measured to be 104 meV. A smaller gap of 45 meV centered around 1.8 eV also appears as the first order air SP and the second order silica SP are excited at the same frequency on opposite sides of the grating.

In order to investigate how the SP dispersion will change in response to changes in the dielectric medium, a second grating was brought in close proximity with the first such that the wires were perpendicular to each other, as shown schematically in Figure 3.4. The second grating had the same period and approximate wire width as the first. To investigate the response of the SP dispersion to the second grating, the dispersion of the bare grating was measured, and then a second grating was pressed to the first such that the wires were perpendicular and facing each other sandwiched between the two silica slides. The dispersion was measured again for the same polarization, as shown in Figure 3.4(b). Finally, the polarization was rotated 45 degrees such that an equal component of the electric field of the incoming light is perpendicular to both gratings, and therefore able to excite a SP on both gratings, as shown in Figure 3.4(c).
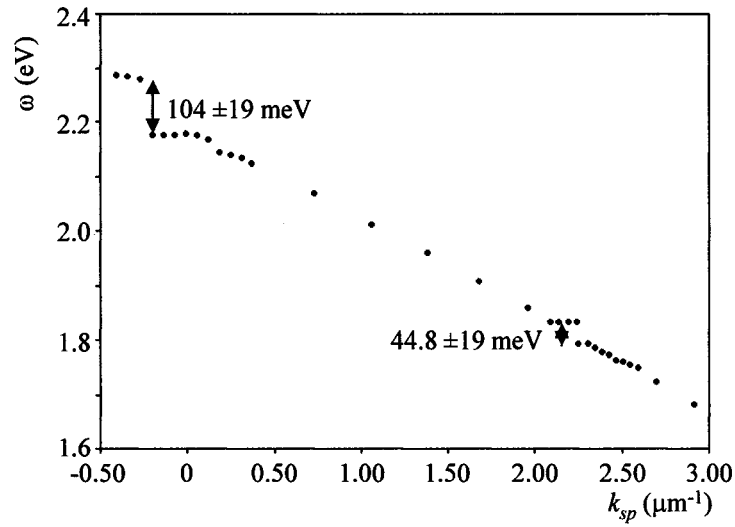
Figure 3.3: Dispersion of bare grating

Dispersion curve showing plasmonic energy gaps of 104 meV as the $\pm 1^{st}$ air side plasmon excited at the same energy. A gap of 45 meV appears as the -1st air side plasmon is excited with the +1 silica side plasmon.
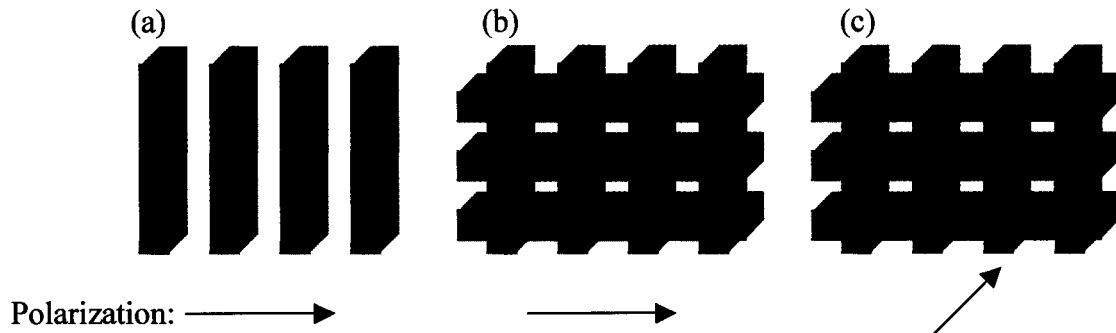
Figure 3.4: Structure and polarization orientation of crossed gratings

(a) Bare grating with p-polarized light. (b) Crossed grating with light p-polarized with respect to the first grating. (c) Crossed grating with light polarized 45° with respect to the first grating.

Because the metal wires are sandwiched between the silica slides, the actual structure cannot be characterized by standard microscopy. However, based on the experimental spectra measured, it is likely that the wires are not in electrical contact with each other because no additional features were present in the spectrum. If the gratings were in electrical contact, additional excitations resulting from the dual periodicity of the system would be observable.[54,72] The second grating was however close enough to strongly influence the dispersion of the SPs of the first grating, as evident in Figure 3.5.

The effect of the second grating is seen in the dispersion curves shown in Figure 3.5. The dispersion curves show the dispersion of the -1st silver-air side SP and focus on the energy gap formed from the SPs excited on opposite sides, here the -1st order air side plasmon and the $+1^{st}$ order silica side plasmon. Initially, there is a 45 meV gap in the dispersion of the bare grating. When the second grating is brought near the first for the same polarization, two changes are seen in the plasmon dispersion. First, the slope decreases indicating that the SPs are propagating more slowly along the metal/dielectric interface. Second, the energy gap widens to 80 meV, indicating a stronger coupling between the two SPs. Because the electric field is only perpendicular to the first grating, SPs are only excited on the first grating. However, if the polarization is rotated 45 degrees, there is a component of the incident electric field perpendicular to both gratings and SPs will be excited on both gratings. Although the slope of the plasmon's dispersion does not change further within experimental error, the energy gap widens to 112 meV, indicating an even stronger coupling between plasmons. Returning to the application of the Kronig-Penney to SPs, the increase in energy gap may be attributed to the presence of

the second grating, which increases the impedance of the surrounding medium. This

effect is amplified when the polarization is rotated and SPs are excited on both gratings.

Structure	Gap	
Grating (p-polarized)	37.1	meV
Crossed Grating (p-polarized)	72.9	meV
Crossed Grating (45°)	113.3	meV

-1 Air Side Plasmon

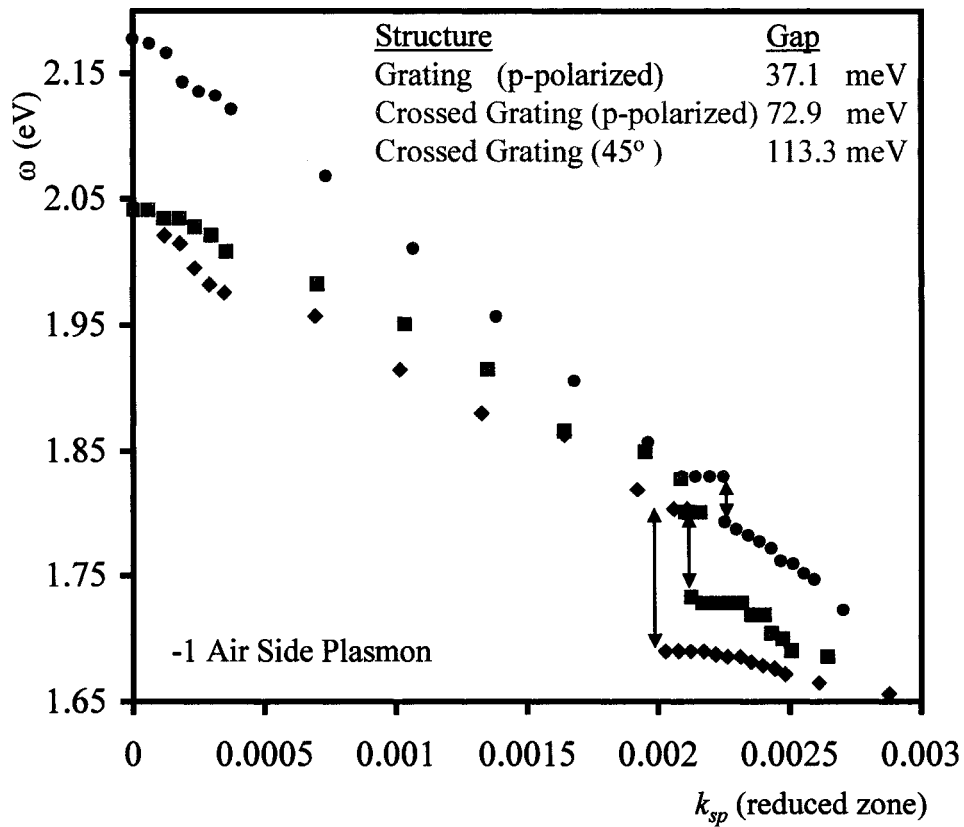k_{sp} (reduced zone)

Figure 3.5: Dispersion curves for crossed gratings.

(Blue) Plasmonic energy gap formed when the -1 air side and +1 silica side plasmon are excited at the same energy. (Red) The energy gap widens from 45 meV to 80 meV and the group velocity is slowed in response to the second grating. (Green) When the polarization is rotated 45°, the energy gap increases further to 112 meV.

3.3 Discussion and Summary

In summary, the effect of bound and unbound dielectric media on SP propagation on metallodielectric gratings has been examined. Measuring the dispersion of SPs excited on gratings yields more information about the SP's character than what is measurable for the localized SP excitations of nanoparticles, namely the group velocity and plasmonic energy gap. Creating a crossed grating structure by placing a second grating perpendicular and in close proximity to a first will decrease the group velocities of the plasmons as well as increase the plasmonic energy gap. Increasing the refractive index of the medium around the wires shifts the dispersion relation to lower energies, decreases the group velocity, and decreases the size of the plasmonic band gap. Conversely, when the refractive index of the nanoscopic environment of the wires is increased by functionalization with an alkanethiol SAM, similar trends are observed for the plasmon energies and group velocities, but the energy gap increases. This increase corresponds to a chemical modification of the metal surface, which increases the potential barrier for SP propagation. This sensitivity to the surrounding medium makes metallodielectric gratings useful in many sensing applications.

Chapter 4: Optical Properties of Nanoshells above a Conducting Plane

Recently there has been much theoretical[47,73,74] and experimental[42,75,76] interest in the interaction between two nanoparticles, or dimers. When nanoparticles are sufficiently close such that their near fields overlap, collective plasmon oscillations between particles are possible.[47,76] The electromagnetic field between the two particles is enhanced because of this interaction.[73] This enhancement is utilized in applications such as surface enhanced Raman scattering (SERS)[29,30] and surface plasmon resonance (SPR) sensing.[43] Most experimental studies on the interactions between particles have been performed on planar particles fabricated on a substrate either by soft lithography[25,26,77,78] or electron beam lithography[30,42,76,79] because of the difficulty in controllably forming dimers between spheroid particles in solution. However, the optical properties of a spherical nanoparticle dimer can be mimicked by a nanoparticle over a conducting plane.[45] When a charged object is placed above a conducting plane, the surface electrons will rearrange themselves such that the resulting electric field is what would result from the charged object and its mirror image. Therefore, the plasmon resonances of a metal nanoparticle above a conducting plane should be similar to a nanoparticle dimer.

The goal of this chapter is to investigate the optical properties of gold nanoshells above a conducting plane and compare the results to what would be expected from a nanoshell dimer. A nanoshell dimer should have both a longitudinal plasmon when the electric field is aligned along the long axis of the dimer and a transverse plasmon when

the electric field is perpendicular to the long axis of the dimer. As the nanoshell plasmon interacts with its image plasmon, two types of plasmon excitations are observed: a longitudinal plasmon orientated perpendicular to the metal surface and a transverse plasmon orientated parallel to the metal surface. By irradiating nanoshell films with polarized light, it will be possible to excite the two possible plasmon orientations separately. Plasmon hybridization is offered as a possible explanation for some of the experimental observations.

4.1 Optical Properties Gold Nanoshells

Gold nanoshells are a silica core surrounded by a thin gold shell fabricated in solution. Because of their core-shell geometry, nanoshells have a tunable plasmon resonance which depends on the ratio of the core radius to the total radius.[22] This tunability can be understood through the plasmon hybridization model.[80,81] Plasmon hybridization separates complex particle systems into their constituent parts and calculates the interaction between the individual plasmon resonances. In the case of a nanoshell, the plasmon resonance of a spherical gold particle is hybridized with a spherical gold cavity to form symmetric and anti-symmetric modes as seen in Figure 4.1. As the thickness of the gold shell is decreased, the interaction between the two plasmons will increase, causing an increased splitting of the symmetric and anti-symmetric modes.[80] This is similar to the case of thin metallic film plasmon modes discussed in Section 2.1.1. This allows the plasmon resonance to be tuned by changing the nanoshell geometry from visible wavelengths to near infrared. The lower energy plasmon, the

ω_+
anti-symmetric

sphere

cavity

ω_- symmetric

$=$ $+$

$\omega_{sp} = \dfrac{\omega_B}{\sqrt{3}}$

$\omega_c = \sqrt{\dfrac{2}{3}}\,\omega_B$

$$\omega_\pm^2 = \frac{\omega_B^2}{2}\left[1 \pm \frac{1}{3}\sqrt{1+8x^3}\right]$$

$x = R_1/R_2$, ω_B = bulk plasmon frequency
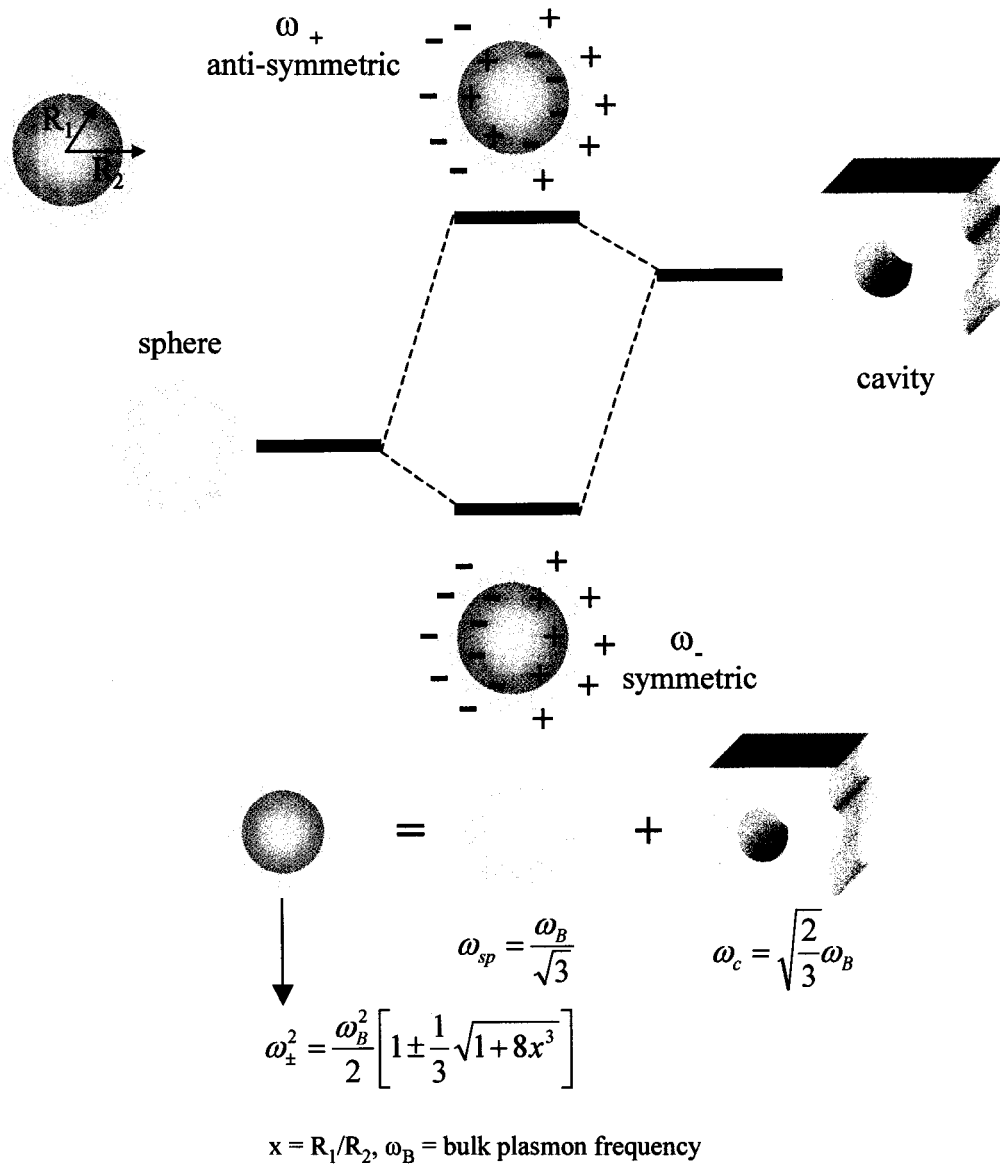
Figure 4.1: Plasmon Hybridization for Gold Nanoshells

Gold nanoshells consist of a silica core of radius R_1 coated by a thin gold shell for a total particle radius of R_2. The plasmon excitations of nanoshells can be thought of as a hybridization of a solid sphere plasmon and a cavity plasmon. If the gold shell is thin, two modes will occur: a higher energy anti-symmetric mode and a lower energy symmetric mode. The splitting, and therefore the energy of the plasmon resonance will depend on the factor R_1/R_2. The symmetric mode is optically active, and therefore what it experimentally measured.

symmetric mode, is the optically active mode and therefore is what is observed experimentally.

4.2 Sample Fabrication and Experimental Setup

Gold is thermally evaporated onto a clean glass slide in a variety of thicknesses ranging from 15-45 nm as measured by a deposition monitor. The thickness of the films was confirmed by atomic force microscopy (AFM) to be within 2 nm of the amount measured. The thinnest films (15 and 25 nm) are not completely continuous according to AFM measurements. The average surface roughness of each film ranged from 0.5 – 2 nm, also as measured by AFM.
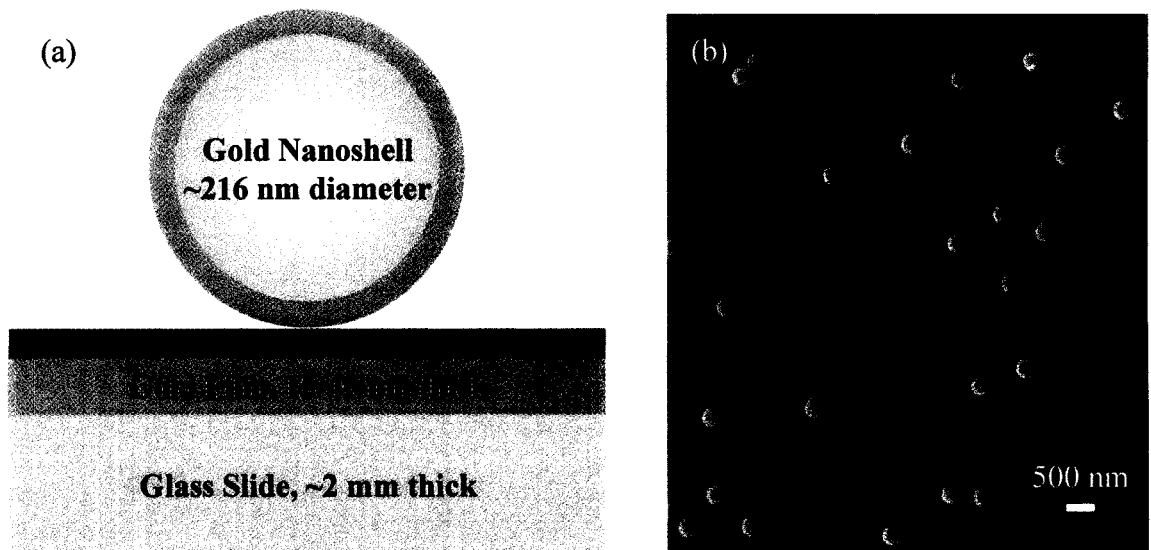

Figure 4.2: Sample Schematic and SEM Micrograph.
(a)   Sample schematic with relevant parameters defined. (b)   SEM micrograph of sample.

Poly(Vinyl Pyridine) (PVP) is used to both immobilize the nanoshells on the surface and prevent aggregation usually present in drop drying deposition techniques. The pyridyl groups of PVP have a strong affinity for metals, making PVP an attractive polymer to facilitate films of well-separated metallic nanoparticles.[82] A layer of PVP is deposited by immersing the glass slides in a 1% by weight ethanolic solution for at least 8 hours. Upon removal from solution, the gold covered glass slides are rinsed with ethanol to remove any unbounded PVP and then dried with a nitrogen stream. Nanoshells are deposited by immersing the functionalized film in an aqueous solution of nanoshells until a well-dispersed film of nanoshells is achieved. Typical deposition times ranged from 15 minutes to 4 hours depending on nanoshell solution concentration. Based on AFM measurements, it is likely that only a monolayer of PVP is present on the gold surface, so the nanoshells are suspended about 1-2 nm off the gold film. The sample geometry can be viewed in Figure 4.2(a).

The nanoshells used in this study have a core radius of 81 nm and a shell thickness of 27 nm. A 30-minute deposition time was used to achieve optimum nanoshell coverage to be measured optically, but separated enough to minimize nanoshell-nanoshell interactions. A SEM micrograph of a typical sample can be seen in Figure 4.2(b). Some dimer and higher order aggregates are present in the nanoshell films, but made up less than 25% of the particles in the films. All extinction spectra were taken using a Cary 5000 UV-VIS spectrophotometer in transmission. Background scans used to calculate the extinction are measured on samples with a PVP functionalized
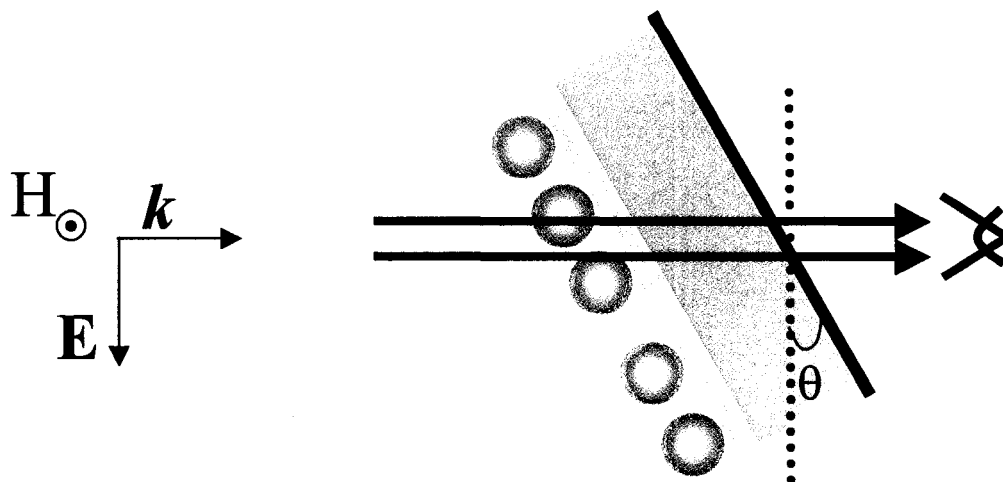
evaporated gold film. The incoming light is p-polarized (magnetic field perpendicular to

the plane of incidence) as shown in Figure 4.3. At normal incidence, the electric field of

Figure 4.3: Experimental Parameters.
p-polarized light is incident on the nanoshell films. Samples are rotated by an angle
θ measured from the sample normal.

the incident light is parallel to the gold film. All measurements were made with the light

incident on the nanoshell side of the sample, however measurements taken with the light

incident on the glass side yielded identical results. The samples are mounted on a

rotation stage, and the angle of rotation, θ, is measured from the sample normal. As the

sample is rotated, a component of the electric field will also be perpendicular to the gold

film. Additionally, as the angle is increased, the spot size on the sample increases. In

order to compare the intensities of spectral features, the spectra are normalized by cos(θ).

The extinction spectra for the nanoshells used as made in an aqueous solution can

be seen in Figure 4.4(a) (red). The dipole resonance appears at 842 nm, and a quadrupole

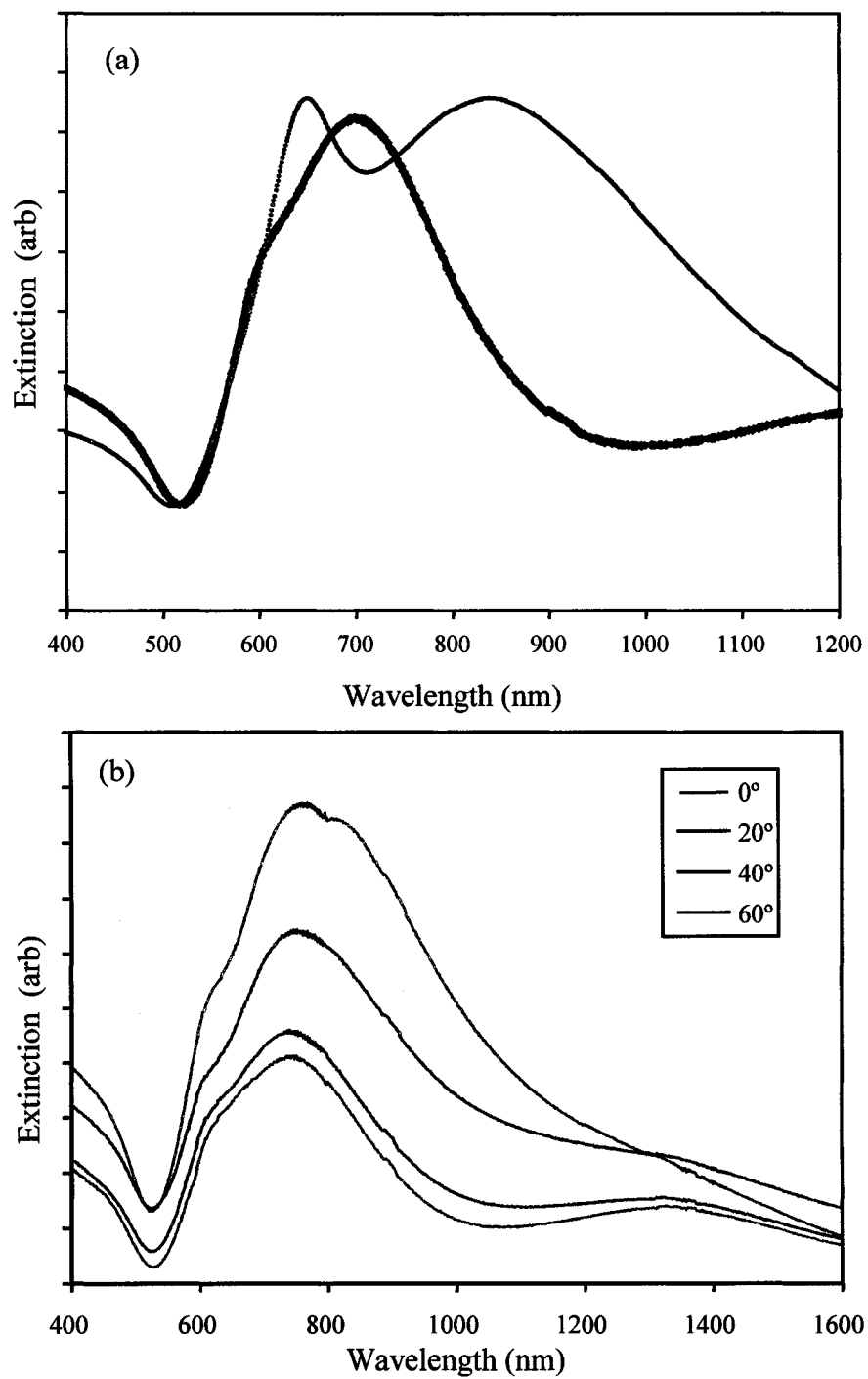peak at 642 nm. Figure 4.4(a) shows the same nanoshells immobilized with PVP on

Figure 4.4: Extinction spectra of Nanoshells.

(a) Extinction spectra of nanoshells used in water (red) and suspended on glass in air (blue). (b) Extinction spectra of nanoshells suspended on glass using p-polarized light incident at different angles

glass in air (blue). Because the index of refraction is reduced from 1.33 in water to 1 in air, the dipole peak shifts to 693 nm and the quadrupole peak to 600 nm. Figure 4.4(b) shows the angle dependent extinction spectra for p-polarized light for nanoshells immobilized with PVP on glass in air. The spectra are shifted for clarity. As the angle is increased, the nanoshell plasmon resonance shifts slightly, but no new features appear in the spectrum. The slight shift in plasmon energy is due to the polarizability of the glass slide.

4.3 Polarization Dependent Image Plasmons

The extinction spectra for the above nanoshells suspended over a 25 nm thick gold film can be seen in Figure 4.5(a). At normal incidence, two peaks labeled (iii) and (ii) can be seen in the spectra at 732 nm and 927 nm respectively. The peak labeled (iii) is very similar in energy to the single nanoshell peak in Figure 4.4. For normal incidence, the electric field is parallel to the surface, exciting parallel plasmon resonances shown schematically in Figure 4.5(b). As the angle of incidence is increased, the intensity of peaks (ii) and (iii) decrease, and new plasmon resonances appear at 1395 nm and 575 nm, labeled as (i) and (iv) respectively. Because these plasmons increase in intensity as the angle of incidence increases, these plasmons may be identified as perpendicular plasmon resonances, shown schematically in Figure 4.5(b).

The plasmon resonance labeled as (i) is the perpendicular dipole plasmon and is lowest in energy because the distance between the nanoshell plasmon electrons and the induced charges in the film is smaller, leading to a stronger interaction. The parallel

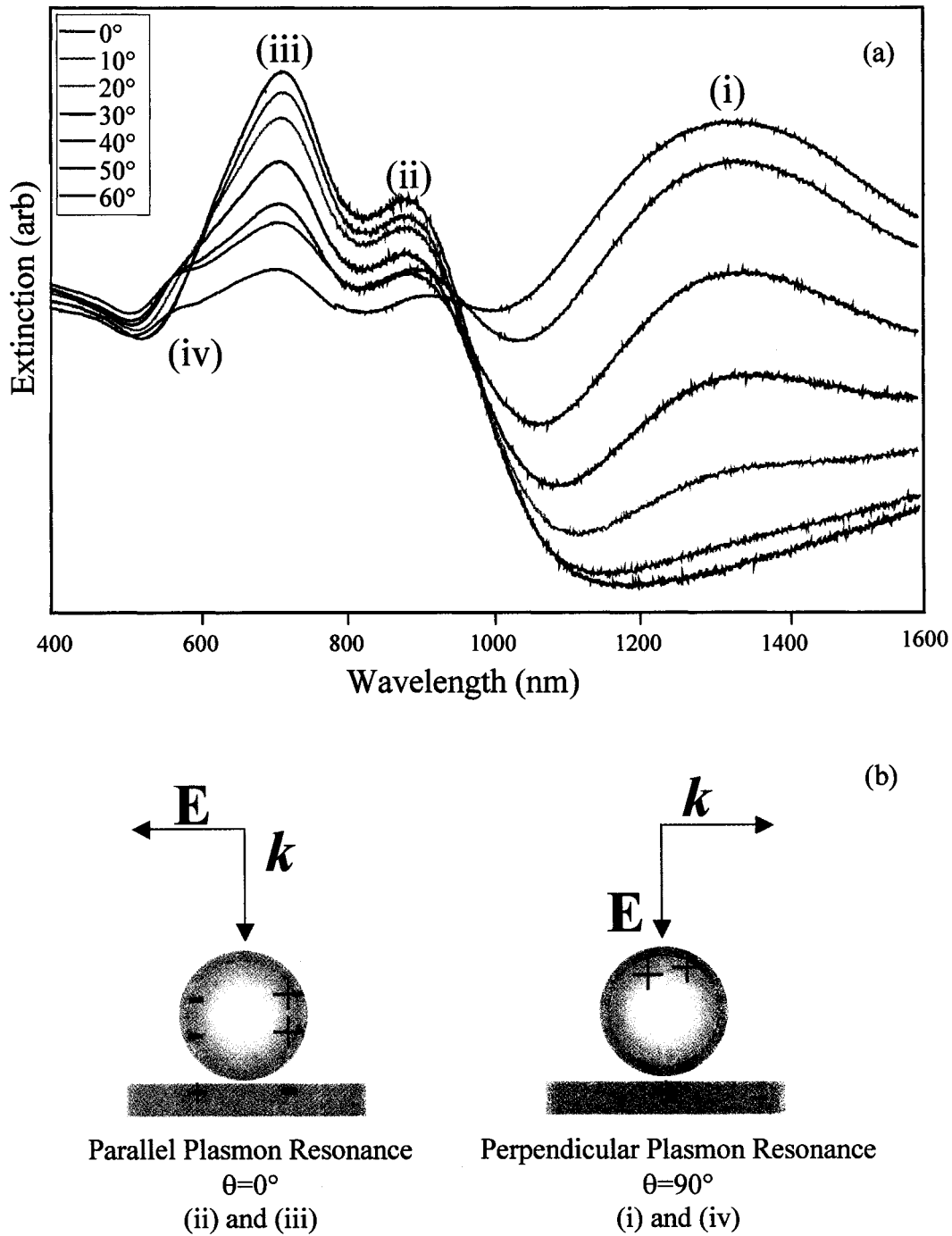**Figure 4.5: Extinction Spectra for Nanoshells over a 25 nm Gold Film.**

(a) Extinction spectra for nanoshells above a 25nm thick gold film as a function of angle. At normal incidence, two parallel plasmon resonances appear, labeled (ii) and (iii). As the angle of incidence is increased, perpendicular plasmon resonances (i) and (iv) appear. (b) charge distributions of parallel and perpendicular plasmon resonances.

plasmons (ii) and (iii) are excited at a higher energy because the displaced electrons of the nanoshell plasmon are further away from the induced electrons on the film surface, therefore the interaction is not as strong. Although it is not possible experimentally, it is likely that if the angle of incidence was rotated 90° only peaks (i) and (iv) would be present. Angles between 0° and 90° are clearly superpositions of the parallel and perpendicular plasmon resonances.

Another experimental parameter that was varied was the thickness of the gold film. Since only surface electrons are involved in creating the image plasmons, it is not clear that changing the film thickness will affect the nanoshell-film plasmon resonances. However, the film thickness clearly influences the energy at which the perpendicular plasmon labeled (i), is excited and to a much lesser extent the parallel plasmons labeled (iii). Figures 4.6(a-d) show the energy at which the nanoshell-film plasmons, (i)-(iv) respectively, are excited as a function of film thickness. There is a clear blue shift in the energy of the perpendicular plasmon resonance labeled (i). There is a slight redshift in the energy of the parallel plasmon resonance labeled (iii). There is no measurable shift in the plasmon resonances labeled (ii) and (iv).
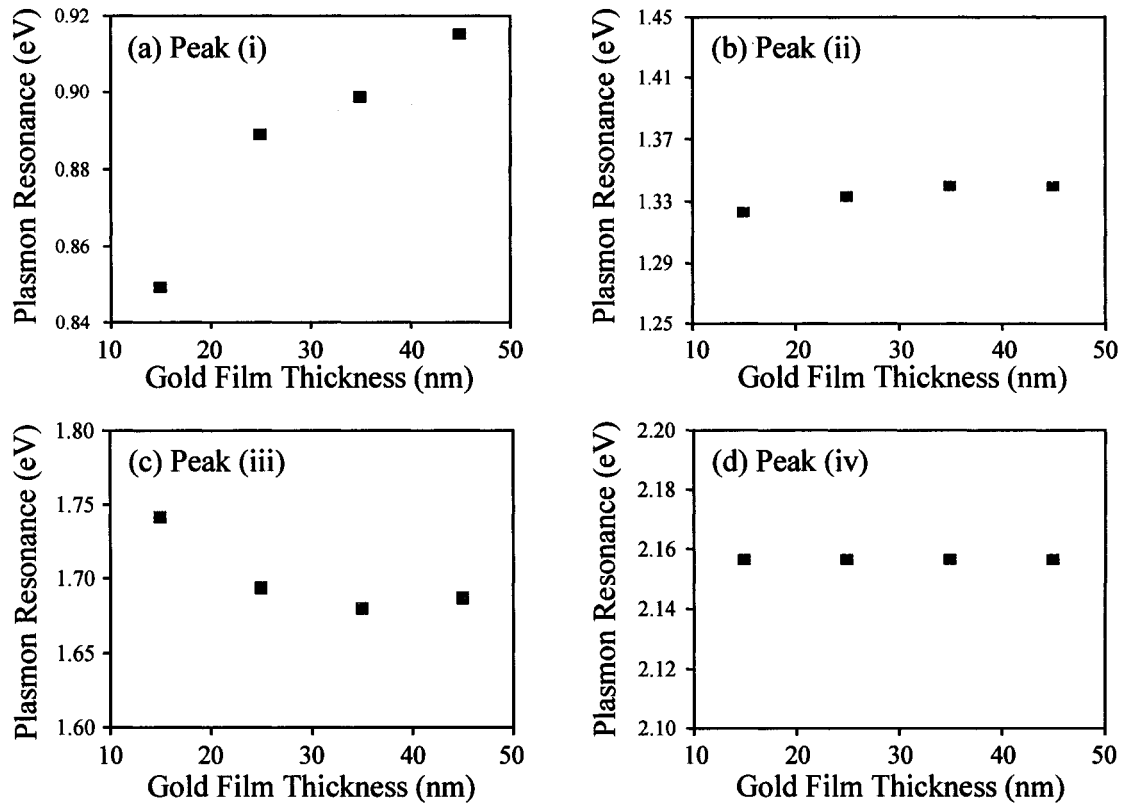
Figure 4.6: Plasmon Resonance Energies versus Film Thickness

Energies of plasmons as labeled (i)-(iv) in Figure 4.5 versus film thickness. (a) The perpendicular plasmon resonance (i) blue shifts with increasing film thickness and is the most sensitive to changed in film thickness. (c) The parallel plasmons resonance (iii) red shifts slightly with increasing film thickness, and the remaining two plasmon resonances (b) and (d) do not change with film thickness.

4.4 Nanoshell-Film Hybridization

Although the simple image charge picture adequately explains the different nanoshell-film plasmons excited, it does not give a complete physical picture of all experimental observations. Because only the surface electrons are involved in the resulting electric field of the nanoshell-film system it is not immediately obvious why the perpendicular plasmon resonance shifts to higher energy with increasing film thickness. However, this affect may be described using the plasmon hybridization model.[80,81] In this case, the plasmon resonances of the thin gold film are hybridized with the nanoshell plasmon.[47] The plasmon resonance of a thin gold film was calculated in Section 2.1.1. The splitting of the high and low energy modes depend on the thickness of the metal as defined in Equation 2.1.12. As the metal becomes thinner, there is a greater splitting of the high and low energy modes. This can also be described using plasmon hybridization as shown in Figure 4.7(a). For thin metal films, the surface plasmon modes excited on each side of the metals interact to form a higher energy anti-symmetric mode and a lower energy symmetric mode. As the films become thinner and the distance between the surface plasmons is decreased, the modes will interact more strongly, increasing the splitting between the modes.

In the case of a nanoshell and a film, the likely coupling is between the symmetric mode of the film and nanoshell shown schematically in Figure 4.7(b). As the film thickness is increased, the thin film plasmon energy increases in energy towards the bulk surface plasmon energy while the nanoshell plasmon remains fixed. As the film plasmon increases in energy, it becomes detuned from the nanoshell plasmon. The film-nanoshell

plasmon will therefore increase in energy in response to the increase film plasmon energy, matching the trend observed for the perpendicular plasmon resonance labeled (i).
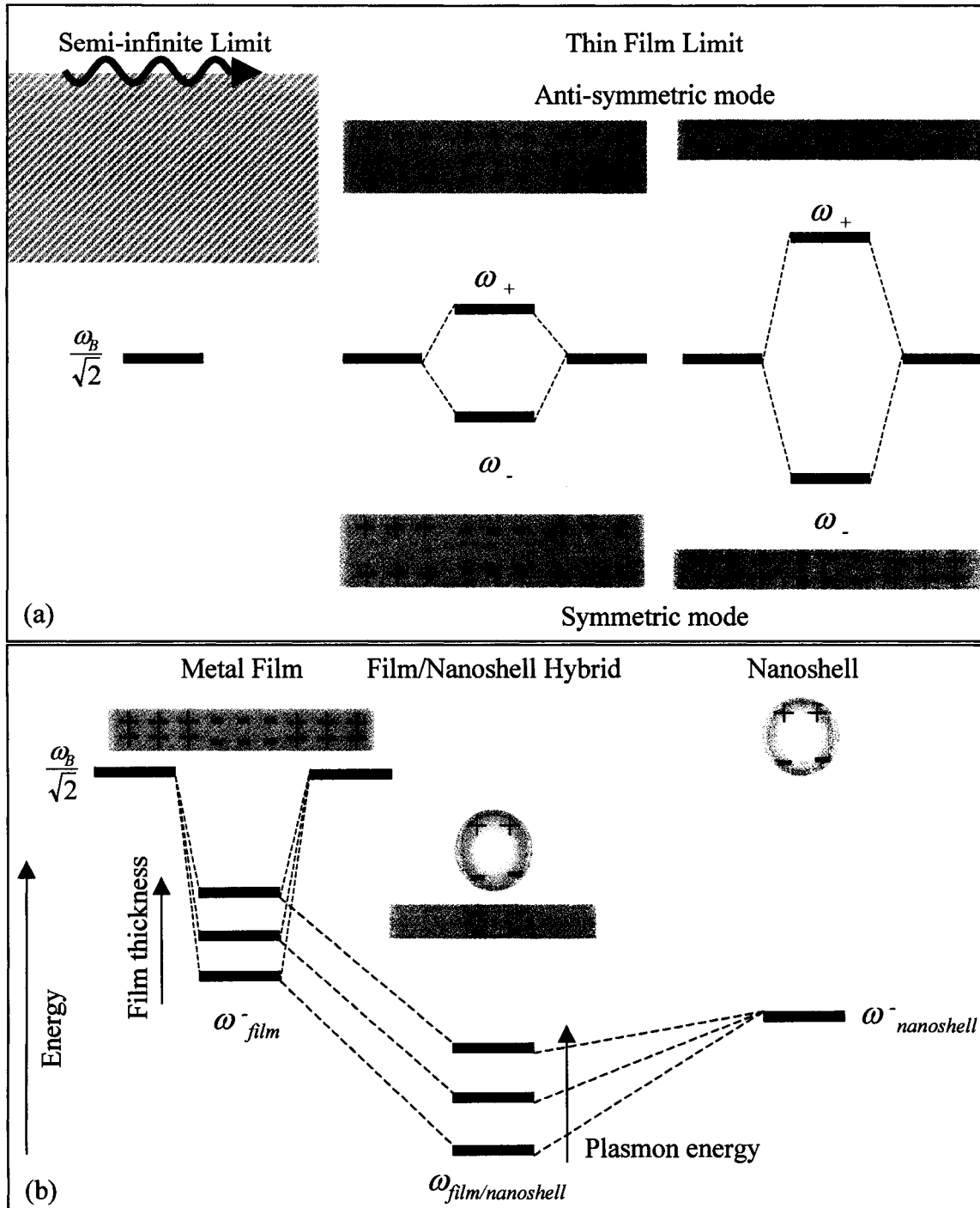
Figure 4.7: Plasmon Hybridization for Metal Film and Nanoshell-Film Geometries

(a) Plasmon hybridization for metal films. As the thickness of the film decreases, the interaction of the plasmons on each side of the film increases causing a greater splitting of the symmetric and anti-symmetric modes. (b) Plasmon hybridization of a thin metal film and nanoshell. As the film becomes thicker, the film plasmon rises in energy, causing the film-nanoshell plasmon energy to also increase.

4.5   Discussion and Summary

This chapter discusses the optical properties of gold nanoshells above a gold film. Two types of plasmon resonances are seen in the transmission spectra: parallel plasmon excitations and perpendicular plasmon excitations, similar to what is expected for a nanoshell dimer system. The perpendicular plasmon has the lowest energy because the induced charges have a smaller separation, causing a strong interaction between the nanoshell plasmon and its image. The parallel plasmons occur at higher energies because of the relatively weaker coupling between the nanoshell plasmon and its image. The energy of the perpendicular plasmon is sensitive to the thickness of the conducting plane. It was found that the energy of the perpendicular plasmon increases with increasing film thickness. This somewhat surprising result can be qualitatively explained using plasmon hybridization theory. As the film thickness increases, the energy of the symmetric film plasmon increases in energy, causing the plasmon energy of the film-nanoshell system to rise as well.

Chapter 5: Conclusions and Future Directions

This thesis investigated the plasmonics of nanostructures in planar geometries. Two geometries were considered: metallodielectric gratings with subwavelength slots and metal nanoshells above a conducting plane. For metallodielectric gratings, the transmission and reflection spectra were measured. Two anomalies were present in the spectra, an 'edge' anomaly occurring when a diffracted order becomes evanescent (termed a Rayleigh anomaly) and a 'diffuse' anomaly that is attributed to surface plasmon excitations. The spectral results were well described by theoretical calculations that utilized a surface impedance boundary condition approximation. Angle resolved measurements yielded the dispersion relations for both Rayleigh anomalies and surface plasmon excitations. A well-defined energy gap was present in the dispersion of the surface plasmons. This energy gap appeared when two counter-propagating surface plasmon interfere to form a standing wave. This occurred not only for counter-propagating surface plasmons excited on the same side of the grating, but also when surface plasmons were excited on opposite sides of the grating. The gratings are sufficiently thin to allow coupling of modes on opposite sides of the grating, similar to thin metallic films.

The plasmonic energy gap arises from the interaction of surface plasmons to form a symmetric (low energy mode) and anti-symmetric (high energy mode) charge distribution on the metal wires with same frequency. Because these modes include an electric charge distribution on the surface of the metal wires coupled to an

electromagnetic field in the surrounding medium, the plasmonic band gap was found to be sensitive to both changes in the surface chemistry of the wire and changes to the surrounding dielectric medium. Three cases were considered, a crossed grating structure, solvent immersion, and chemical functionalization. For the first two cases, the plasmonic energy gap decreased in response to the change in dielectric medium. Specifically for solvent immersion, as the surrounding index of refraction increased, the plasmonic energy gap decreased. However, for chemical functionalization, the plasmonic energy gap increased. These two opposing trends were qualitatively explained by comparing plasmons traveling on a metallodielectric grating to electrons traveling in a periodic potential through the Kronig-Penney model.

The effect of chemical functionalization was only explored in detail for two lengths of alkanethiols. A logical next step would be to investigate alkanethiols of different carbon chain lengths and molecules that bond differently to metals such as amine terminated carbon chains. It would also be interesting to coat a grating in a thin dielectric layer not chemically bound to the metal wires as a comparison to molecular SAMs.

The second geometry considered was a metal nanoshell above a thin conducting plane. Gold nanoshells were suspended above a gold film using a PVP spacer layer. The nanoshell is close enough to the metal film so that it can interact with its image plasmon, mimicking a nanoshell dimer. The optical properties in transmission were measured as a function of polarization angle. Plasmon resonances aligned both parallel and perpendicular to the gold film were excited, similar to what is expected for a nanoshell dimer. The thickness of the gold film was also varied. As the film thickness increased, a

blue shift in energy was found for the plasmon excited perpendicular to the gold film. This somewhat surprising result was qualitatively explained through the plasmon hybridization model. This model considers how the nanoshell plasmons couple to the film surface plasmons. Because the gold film is thin, the surface plasmons were split into two modes: a lower energy symmetric mode and a higher energy anti-symmetric mode. The nanoshell plasmon most likely interacts with the lower energy mode of the film. As the film thickness is increased, this mode will increase in energy until it reaches the bulk film value. As the film energy level rises, the hybrid nanoshell-film plasmon rises as well, resulting in a blue shift in plasmon energies.

There are many issues this research has raised that should be answered in the future. First, simple variations in the nanoshell-substrate geometry could be made. For example, varying the distance of the nanoshell from the metal film should detune the nanoshell and film plasmons until they are non-interacting. This would provide insight into the length scales important to these interactions. Second, the material of the conducting plane can be varied, for example, aluminum should be a particularly interesting case. Aluminum is a good conductor, and therefore from the standpoint of simple image charge theory should be able to easily create a nanoshell image plasmon. But, aluminum has a very weak plasmon resonance, and therefore from a plasmon hybridization model standpoint the interaction between the nanoshell and the substrate should be very weak. Finally, as nanoparticles are introduced in opto-electronic applications, and therefore into the planar geometries such as computer chips, how nanoshells or other nanoparticles interact with a semiconducting substrate will become increasingly important.

Bibliography

1.   Wood, R. W. *Philosophical Magazine* 4, 396 (1902).

2.   Wood, R. W. Anomalous Diffraction Gratings. *Physical Review* 48, 928-936 (1935).

3.   Rayleigh. *Philosophical Magazine* 14, 60 (1907).

4.   Fano, U. The Theory of Anomalous Diffraction Gratings and of Quasi-Stationary Waves on Metallic Surfaces (Sommerfeld's Waves). *Journal of the Optical Society of America* 31, 213-222 (1941).

5.   Raether, H. R. *Surface Plasmons on Smooth and Rough Surfaces and on Gratings* (Springer-Verlag, New York, 1988).

6.   Stewart, J. E. & Gallaway, W. S. Diffraction Anomalies in Grating Spectrophotometers. *Applied Optics* 1, 421-429 (1962).

7.   Hutley, M. C. An experimental study of the anomalies of sinusoidal diffraction gratings. *Optica Acta* 20, 607-624 (1973).

8.   Hutley, M. C. & Bird, V. M. A detailed experimental study fo the anomalies of a sinusoidal diffraction grating. *Optica Acta* 20, 771-782 (1973).

9.   Schroter, U. & Heitmann, D. Grating couplers for surface plasmons excited on thin metal films in the Kretschmann-Raether configuration. *Physical Review B* 60, 4992-4999 (1999).

10. Pockrand, I. Resonance anomalies in the light intensity reflected at silver gratings with dielectric coatings. *Journal of Physics D* 9, 2423-2432 (1976).

11. Lochbihler, H. Surface polaritons on metallic wire gratings studied via power losses. *Phys. Rev. B* 53, 10289 - 10295 (1996).

12. Lochbihler, H. & Depine, R. Highly conducting wire gratings in the resonance region. *Applied Optics* 32, 3459-3465 (1993).

13. Lochbihler, H. & Depine, R. A. Characterization of highly conducting wire gratings using an electromagnetic theory of diffraction. *Optics Communications* 1000, 231-239 (1993).

14. Lochbihler, H. Surface polaritons on gold-wire gratings. *Physical Review B* 50, 4795-4801 (1994).

15. Steele, J. M., Moran, C.E., Lee, A., Aguirre, C.M. & Halas, N.J. Metallodielectric gratings with subwavelength slots: Optical properties. *Physical Review B* 68, 205103 (2003).

16. Cao, Q. & Lalanne, P. Negative role of surface plasmons in the transmission of metallic gratings with very narrow slits. *Physical Review B* 88, 057403-1-4 (2002).

17. Porto, J. A., Garcia-Vidal, F. J. & Pendry, J. B. Transmission resonances on metallic gratings with very narrow slits. *Physical Review Letters* 83, 2845-2848 (1999).

18. Garcia-Vidal, F. J. & Pendry, J. B. Collective Theory for Surface Enhanced Raman Scattering. *Physical Review Letters* 77, 1163-1166 (1996).

19.   Mie, G. *Ann. Phys.* 25, 377 (1908).

20.   Bohren, C. F. & Huffman, D. R. *Absorption and Scattering of Light by Small Particles* (ed. Series, W. S. P.) (John Wiley and Sons, Inc, New York, 1983).

21.   Kreibig, U. & Vollmer, M. *Optical Properties of Metal Clusters* (Springer-Verlag, 1995).

22.   Oldenburg, S. J., Averitt, R. D., Westcott, S. L. & Halas, N. J. Nanoengineering of optical resonances. *Chemical Physics Letters* 288, 243-247 (1998).

23.   Nikoobakht, B. & El-Sayed, M. A. Preparation and Growth Mechanism of Gold Nanorods (NRs) Using Seed-Mediated Growth Method. *Chemistry of Materials* 15, 1957-1962 (2003).

24.   Charnay, C. et al. Reduced symmetry metallodielectric nanoparticles: Chemical synthesis and plasmonic properties. *Journal of Physical Chemistry B* 107, 7327-7333 (2003).

25.   Jensen, T. R., Duyne, R. P. V., Johnson, S. A. & Maroni, V. A. Surface-enhanced infrared spectroscopy: A comparison of metal island films with discrete and nondiscrete surface plasmons. *Applied Spectroscopy* 54, 371-377 (2000).

26.   Jensen, T. R., Schatz, G. C. & Van Duyne, R. P. Nanosphere lithography: Surface plasmon resonance spectrum of a periodic array of silver nanoparticles by ultraviolet-visible extinction spectroscopy and electrodynamic modeling. *Journal of Physical Chemistry B* 103, 2394-2401 (1999).

27.   Sun, Y. G. & Xia, Y. N. Increased sensitivity of surface plasmon resonance of gold nanoshells compared to that of gold solid colloids in response to environmental changes. *Analytical Chemistry* 74, 5297-5305 (2002).

28.   Salerno, M. et al. Near-field optical response of a two-dimensional grating of gold nanoparticles. *Physical Review B* 6316, 165422 (2001).

29.   Gunnarsson, L. et al. Interparticle coupling effects in nanofabricated substrates for surface-enhanced Raman scattering. *Applied Physics Letters* 78, 802-804 (2001).

30.   Felidj, N. et al. Controlling the optical response of regular arrays of gold particles for surface-enhanced Raman scattering. *Physical Review B* 65 (2002).

31.   Kneipp, K., Kneipp, H., Itzkan, I., Dasari, R. R. & Feld, M. S. Ultrasensitive chemical analysis by Raman spectroscopy. *Chemical Reviews* 99, 2957 - 2975 (1999).

32.   Jackson, J. B., Westcott, S. L., Hirsch, L. R., West, J. L. & Halas, N. J. Controlling the surface enhanced Raman effect via the nanoshell geometry. *Applied Physics Letters* 82, 257-259 (2003).

33.   Haynes, C. L. & Van Duyne, R. P. Plasmon-sampled surface-enhanced Raman excitation spectroscopy. *Journal of Physical Chemistry B* 107, 7426-7433 (2003).

34.   Hutter, E. et al. Role of substrate metal in gold nanoparticle enhanced surface plasmon resonance imaging. *Journal of Physical Chemistry B* 105, 8-12 (2001).

35.   He, L. et al. Colloidal Au-enhanced surface plasmon resonance for ultrasensitive detection of DNA hybridization. *Journal of the American Chemical Society* 122, 9071-9077 (2000).

36.   Malinsky, M. D., Kelly, K. L., Schatz, G. C. & Van Duyne, R. P. Chain length dependence and sensing capabilities of the localized surface plasmon resonance of silver nanoparticles chemically modified with alkanethiol self-assembled monolayers. *Journal of the American Chemical Society* 123, 1471-1482 (2001).

37.   Haynes, C. L. & Van Duyne, R. P. Nanosphere lithography: A versatile nanofabrication tool for studies of size-dependent nanoparticle optics. *Journal of Physical Chemistry B* 105, 5599-5611 (2001).

38.   Barnes, W. L., Dereux, A. & Ebbesen, T. W. Surface plasmon subwavelength optics. *Nature* 424, 824-830 (2003).

39.   Ditlbacher, H., Krenn, J. R., Schider, G., Leitner, A. & Aussenegg, F. R. Two-dimentional optics with surface plasmon polaritons. *Applied Physics Letters* 81, 1762 (2002).

40.   Maier, S. A. et al. Plasmonics - A Route to Nanoscale Optical Devices. *Advanced Materials* 13, 1501 (2001).

41.   Soller, B. J. & Hall, D. G. Direct observation of a propagating, planar-waveguide surface mode in a discontinuous film of metal nanoparticles. *Optics Letters* 25, 1071-1073 (2000).

42.   Felidj, N. et al. Enhanced substrate-induced coupling in two-dimensional gold nanoparticle arrays. *Physical Review B* 66 (2002).

43.   Hutter, E., Fendler, J. H. & Roy, D. Surface plasmon resonance studies of gold and silver nanoparticles linked to gold and silver substrates by 2-aminoethanethiol

and 1,6-hexanedithiol. *Journal of Physical Chemistry B* 105, 11159-11168 (2001).

44.   Malinsky, M. D., Kelly, K. L., Schatz, G. C. & Van Duyne, R. P. Nanosphere lithography: Effect of substrate on the localized surface plasmon resonance spectrum of silver nanoparticles. *Journal of Physical Chemistry B* 105, 2343-2350 (2001).

45.   Okamoto, T. & Yamaguchi, I. Optical absorption study of the surface plasmon resonance in gold nanoparticles immobilized onto a gold substrate by self-assembly technique. *Journal of Physical Chemistry B* 107, 10321-10324 (2003).

46.   Ruppin, R. Optical-Absorption of a Coated Sphere above a Substrate. *Physica A* 178, 195-205 (1991).

47.   Gozhenko, V. V., Grechko, L. G. & Whites, K. W. Electrodynamics of spatial clusters of spheres: Substrate effects. *Physical Review B* 68, 125422 (2003).

48.   Astilean, S., Lalanne, P. & Palamaru, M. Light transmission through metallic channels much smaller than the wavelength. *Optics Communications* 175, 265-273 (2000).

49.   Collin, S., Pardo, F., Teissier, R. & Pelouard, J.-L. Horizontal and vertical surface resonances in transmission metallic gratings. *Journal of Optics A* 4, S154-S160 (2002).

50.   Barbara, A., Quemerais, P., Bustarret, E. & Lopez-Rios, T. Optical transmission through subwavelength metallic gratings. *Physical Review B* 66, 161403-161403-4 (2002).

51.   Garcia-Vidal, F. J. & Martin-Moreno, L. Transmission and focusing of light in one-dimensional periodically nanostructured metals. *Physical Review B* 66, 155412-1-10 (2002).

52.   Stavrinou, P. N. & Solymar, L. The propagation of electromagnetic power through subwavelength slits in a metallic grating. *Optics Communications* 206, 217-223 (2002).

53.   Ebbesen, T. W., Lezec, H. J., Ghaemi, H. F., Thio, T. & Wolf, P. A. Extraordinary optical transmission through sub-wavelength hole arrays. *Nature* 391, 667-669 (1998).

54.   Ghaemi, H. F., Thio, T., Grupp, D. E., Ebbesen, T. W. & Lezec, H. J. Surface plasmons enhance optical transmission through subwavelength holes. *Physical Review B* 58, 6779-6782 (1998).

55.   Popov, E., Neviere, M., Enoch, S. & Reinisch, R. Theory of light transmission through subwavelength periodic hole array. *Physical Review B* 62, 16100-16108 (2000).

56.   Collin, S., Pardo, F., Teissier, R. & Pelouard, J.-L. Strong discontinuities in the complex photonic band structure of transmission metallic gratings. *Physical Review B* 63, 033107-1-4 (2001).

57.   Barnes, W. L., Preist, T. W., Kitson, S. C. & Sambles, J. R. Physical origin of photonic energy gaps in the propagation of surface plasmons on gratings. *Physical Review B* 54, 6227-6244 (1996).

58.   Moran, C. E., Radloff, C. & Halas, N. J. Benchtop fabrication of submicrometer metal line and island Arrays using passivative microcontact printing and electroless plating. *Advanced Materials* 15, 804-+ (2003).

59.   Weber, M. G. & Mills, D. L. Determination of surface-polariton minigaps on grating structures: A comparison between constant-frequency and constant-angle scans. *Physical Review B* 34, 2893-2894 (1986).

60.   Depine, R. A. & Simon, J. M. Surface impedance boundary condition for metallic diffraction gratings in the optical and infrared range. *Optica Acta* 30, 313-322 (1983).

61.   Lochbihler, H. & Depine, R. Highly conduction wire gratings in the resonance region. *Applied Optics* 32, 3459-3465 (1993).

62.   Johnson, P. B. & Christy, R. W. Optical Constants of the Noble Metals. *Physical Review B* 6, 4370-4379 (1972).

63.   Bailey, R. C., Nam, J. M., Mirkin, C. A. & Hupp, J. T. Real-time multicolor DNA detection with chemoresponsive diffraction gratings and nanoparticle probes. *Journal of the American Chemical Society* 125, 13541-13547 (2003).

64.   Haes, A. J., Zou, S. L., Schatz, G. C. & Van Duyne, R. P. A nanoscale optical biosensor: The long range distance dependence of the localized surface plasmon resonance of noble metal nanoparticles. *Journal of Physical Chemistry B* 108, 109-116 (2004).

65.   Yonzon, C. R., Haynes, C. L., Zhang, X. Y., Walsh, J. T. & Van Duyne, R. P. A glucose biosensor based on surface-enhanced Raman scattering: Improved

partition layer, temporal stability, reversibility, and resistance to serum protein interference. *Analytical Chemistry* 76, 78-85 (2004).

66.   Tam, F. & Halas, N. Plasmon response of nanoshell dopants in organic films: a simulation study. *Progress in Organic Coatings* 47, 275-278 (2003).

67.   Moran, C. E., Steele, J. M. & Halas, N. J. Chemical and dielectric manipulation of the plasmonic band gap of metallodielectric arrays. *submitted* (2004).

68.   Ashcroft, N. W. & Mermin, N. D. *Solid State Physics* (Saunders College Publishing, New York, 1976).

69.   Linnert, T., Mulvaney, P. & Henglein, A. Surface chemistry of collodial silver: Surface plasmon damping by chemisorbed I, SH, and C6H5S. *Journal of Physical Chemistry* 97, 679-682 (1993).

70.   Henglein, A. Physicochemical properties of small metal particles in solution: "Microelectrode" reactions, chemisorption, composite metal particles, and the atom-to-metal transition. *Journal of Physical Chemistry* 97, 5457-5471 (1993).

71.   Haes, A. J. & Van Duyne, R. P. A nanoscale optical biosensor: Sensitivity and selectivity of an approach based on the localized surface plasmon resonance spectroscopy of triangular silver nanoparticles. *Journal of the American Chemical Society* 124, 10596-10604 (2002).

72.   Minhas, B. K., Fan, W., Agi, K., Brueck, S. R. J. & Malloy, K. J. Metallic inductive and capacitive grids: theory and experiment. *Journal of the Optical Society of America A* 19, 1352-1359 (2002).

73.   Hao, E. & Schatz, G. C. Electromagnetic fields around silver nanoparticles and dimers. *Journal of Chemical Physics* 120, 357-366 (2004).

74.   Kottmann, J. P. & Martin, O. J. F. Retardation-induced plasmon resonances in coupled nanoparticles. *Optics Letters* 26, 1096-1098 (2001).

75.   Stuart, H. R. & Hall, D. G. Enhanced dipole-dipole interaction between elementary radiators near a surface. *Physical Review Letters* 80, 5663-5666 (1998).

76.   Rechberger, W. et al. Optical properties of two interacting gold nanoparticles. *Optics Communications* 220, 137-141 (2003).

77.   Hulteen, J. C. et al. Nanosphere lithography: Size-tunable silver nanoparticle and surface cluster arrays. *Journal of Physical Chemistry B* 103, 3854-3863 (1999).

78.   Jensen, T. R., Malinsky, M. D., Haynes, C. L. & Van Duyne, R. P. Nanosphere lithography: Tunable localized surface plasmon resonance spectra of silver nanoparticles. *Journal of Physical Chemistry B* 104, 10549-10556 (2000).

79.   Felidj, N. et al. Optimized surface-enhanced Raman scattering on gold nanoparticle arrays. *Applied Physics Letters* 82, 3095-3097 (2003).

80.   Prodan, E. & Nordlander, P. Plasmon hybridization in spherical nanoparticles. *Journal of Chemical Physics* 120, 5444-5454 (2004).

81.   Prodan, E., Radloff, C., Halas, N. J. & Nordlander, P. A hybridization model for the plasmon response of complex nanostructures. *Science* 302, 419-422 (2003).

82.   Malynych, S., Luzinov, I. & Chumanov, G. Poly(vinyl pyridine) as a universal surface modifier for immobilization of nanoparticles. *Journal of Physical Chemistry B* 106, 1280-1285 (2002).

Appendix A: Metal Wire Grating Code Library

The following is an outline of the programs that implement the Surface Impedance Boundary Condition approach for calculating the electromagnetic fields diffracted by metal wire gratings as described by Lochbihler and Depine in *Applied Optics*, Volume 32 Issue 19, page 3459 in 1993. The programs were written for Matlab, and are listed with their input variables and subprograms.

I.   Main Programs

gratecompwrap.m: wrapper program that sets experimental parameters and calls the main program, gratingcomp.m. Parameters entered in gratecompwrap.m include the number of modes in the expansion in the grooves of the wires, number of Rayleigh modes in the expansion above and below the wires, the physical size of the gratings, the range of wavelengths, the angle of incident radiation, the polarization of incident radiation, the dielectric functions of the wires and surrounding mediums, and the desired accuracy. The inputs are entered directly in the program, and are therefore not prompted.

gratingcomp.m: calculates the reflection and transmission coefficients for the Rayleigh expansion of the electromagnetic fields as well as the reflected and transmitted power for metal wire gratings. The program calls the following subprograms:

ProporevanT.m and proporevanR.m: determines if a reflected (proporevanR) or transmitted (proporevanT) diffracted order is propagating or evanescent.

I_mmS.m, K_jnS.m, J_qmS.m, and Q_qnS.m: integral matrix elements that correspond to equations (29), (33), (35) and (36) in Lochbihler and Depine respectively.

II.   Visualization Programs

The near fields of the reflected and transmitted electromagnetic field were visualized by the following programs:

gratingvis.m: calculates the components of the electric and magnetic fields in the regions above (reflected radiation) and below (transmitted radiation) the wires. Gratingvis.m calls the following programs:

Rayleighupper.m and Rayleighlower.m: evaluates the electromagnetic fields for the regions above (Rayleighupper.m) and below (Rayleighlower.m) the wire gratings.

III.   Other Programs

Rayleighfinder.m: finds Rayleigh anomalies, or the wavelength for a specified angle of incidence will become evanescent for a certain set of grating parameters.